TKK Dissertations 6
Espoo 2005

APPROACHES FOR MODELLING AND RECONSTRUCTION IN OPTICAL TOMOGRAPHY IN THE PRESENCE OF ANISOTROPIES

Doctoral Dissertation

Jenni Heino

Helsinki University of Technology
Department of Engineering Physics and Mathematics
Laboratory of Biomedical Engineering

TKK Dissertations 6
Espoo 2005

APPROACHES FOR MODELLING AND RECONSTRUCTION IN OPTICAL TOMOGRAPHY IN THE PRESENCE OF ANISOTROPIES

Doctoral Dissertation

Jenni Heino

Dissertation for the degree of Doctor of Science in Technology to be presented with due permission of the Department of Engineering Physics and Mathematics for public examination and debate in Auditorium F1 at Helsinki University of Technology (Espoo, Finland) on the 20th of May, 2005, at 12 noon.

Helsinki University of Technology
Department of Engineering Physics and Mathematics
Laboratory of Biomedical Engineering

Teknillinen korkeakoulu
Teknillisen fysiikan ja matematiikan osasto
Lääketieteellisen tekniikan laboratorio

Distribution:
Helsinki University of Technology
Department of Engineering Physics and Mathematics
Laboratory of Biomedical Engineering
P.O.Box 2200
FI - 02015 TKK
FINLAND
Tel. +358-(0)9-451 3172
fax +358-(0)9-451 3182
URL: http://biomed.tkk.fi/
E-mail: Jenni.Heino@tkk.fi

ISBN 951-22-7668-2
ISBN 951-22-7669-0 (PDF)
ISSN 1795-2239
ISSN 1795-4584 (PDF)
URL: http://lib.tkk.fi/Diss/2005/isbn9512276690/

TKK-DISS-1996

Otamedia Oy
Espoo 2005

HELSINKI UNIVERSITY OF TECHNOLOGY P.O. BOX 1000, FI-02015 TKK http://www.tkk.fi	ABSTRACT OF DOCTORAL DISSERTATION

Author Jenni Heino

Name of the dissertation

Approaches for modelling and reconstruction in optical tomography in the presence of anisotropies

Date of manuscript January 25, 2005	Date of the dissertation May 20, 2005
☐ Monograph	☑ Article dissertation (summary + original articles)

Department	Department of Engineering Physics and Mathematics
Laboratory	Laboratory of Biomedical Engineering
Field of research	Medical imaging, inverse problems
Opponent(s)	Dr. Arnold D. Kim
Supervisor	Prof. Toivo Katila
(Instructor)	Prof. Erkki Somersalo

Abstract

In this thesis, models for light propagation and solution methods for the inverse problem in medical optical tomography (OT) in the presence of anisotropies are developed. Light propagation is modelled using the anisotropic diffusion equation (DE) in the frequency domain. The derivation of the diffusion equation in an anisotropic case is sketched, and the relevant boundary and source conditions presented. The numerical solution is obtained using the finite element (FE) method. The numerical work is done in two dimensional space in order to facilitate the testing of the novel methods for solving the inverse problem. To verify the light propagation model, the 2D FE solution is compared to the boundary element method solution to the DE and to a Monte Carlo simulation.

The main emphasis is on the solution of the inverse problem in OT in the presence of anisotropies. The anisotropic inverse problem is non-unique, and hence simultaneous reconstruction of both the anisotropic diffusion tensor and the absorption coefficient is not feasible without substantial prior knowledge. The goal in this work is to reconstruct the spatial distribution of the optical absorption coefficient and overcome the disturbing effect of the background anisotropies. At the same time, the prior knowledge available on the anisotropies is assumed to be rather limited. A few different approaches for estimating the absorption coefficient is presented. Firstly, an attempt to use a conventional isotropic reconstruction scheme is considered. In this case, the obtained estimates suffer from relative large artefacts. In the second approach the structure of the anisotropy is assumed known, and the spatially constant strength is reconstructed simultaneously with the absorption. The quality of the absorption estimate degrades quickly with the accuracy of the underlying anisotropy structure. To help this, statistical inversion methods are employed. Statistical methods provide means to model the prior information on unknown parameters through probability distributions. The anisotropy parameters are modelled using relatively loose Gaussian priors. By using Gaussian priors the posterior probability distribution of the absorption on condition of the measurements also assumes a Gaussian form. Hence the conditional mean estimates and covariances can be derived in a closed form without having to resort to numerical integration. The statistical approach is used to derive a modelling error approach, where the effect of anisotropies is treated as a modelling error and included into estimation. Implementing the statistical inversion methods enables recovering the main features in the absorption distribution. The statistical treatment of anisotropies is also applied to help the inverse problem when the boundary shape and source/measurement locations are modelled inaccurately.

Keywords Optical tomography, medical imaging, anisotropies, inverse problems, finite elements

Number of pages 185	ISBN (printed) 951-22-7668-2
ISBN (pdf) 951-22-7669-0	ISBN (others)
ISSN (printed) 1795-2239	ISSN (pdf) 1795-4584

Publisher Laboratory of Biomedical Engineering, Helsinki University of Technology

Print distribution Laboratory of Biomedical Engineering, Helsinki University of Technology

☑ The dissertation can be read at http://lib.tkk.fi/Diss/ 2005/isbn9512276690/

Preface

This work has been carried out in the Laboratory of Biomedical Engineering (BME), Helsinki University of Technology. Part of the work has also been done in co-operation with Professor Simon Arridge during my visits to University College London. The financial support from the Academy of Finland, the Finnish Cultural Foundation, the Foundation of Technology (TES), the Jenny and Antti Wihuri Foundation, the Emil Aaltonen Foundation, the Magnus Ehrnrooth Foundation, and the National Technology Agency of Finland (TEKES) is gratefully acknowledged.

I would like to thank my supervisor Professor Toivo Katila for providing excellent conditions for this research and for his support. I would like to express my deepest gratitude to my instructor Professor Erkki Somersalo for the ideas, guidance and support for this research, as well as for arranging the funding for the latter part of this work.

I wish to thank my pre-examiners Dr. Marko Vauhkonen and Dr. Colin Fox for carefully reading the manuscript.

I would like to thank the research group in BME for the nice atmosphere at work. Especially, I want to thank Dr. Ilkka Nissilä for the useful discussions on optical imaging and measurements as well as some practical help. Tommi Noponen also deserves thanks for his help on some practical issues, and the aforementioned two and Dr. Timo Kajava for reading and commenting the manuscript.

I am much in debt to Professor Simon Arridge from UCL for welcoming me to visit UCL at several occasions and for his ideas and advice. I would also like to thank Professor Jan Sikora for the BEM calculations and the whole Medical Image Processing Group at UCL for the friendly working environment.

I would like to thank Professor Jari Kaipio for his ideas and support. I am also grateful to Dr. Jukka Nenonen for his support at the early stages of my work and Dr. Seppo Järvenpää for the mesh generation program used to create the meshes in this work. I also thank Juha Heiskala for his communications on Monte Carlo simulations in head models.

I would also like to express my appreciation to people in the Finnish Inverse Problems Society as well as all the rest of my colleagues for the beneficial and friendly interactions.

Finally, I want to express my gratitude to my friends for all the relaxed moments and my parents Ritva and Veikko for their constant support.

Espoo, April 2005

Jenni Heino

Contents

List of publications

This thesis consist of an overview and the following six publications:

I Jenni Heino and Erkki Somersalo "Estimation of optical absorption in anisotropic background" *Inverse Problems* **18** 559-573 (2002).

II Jenni Heino, Simon Arridge, Jan Sikora, and Erkki Somersalo "Anisotropic effects in highly scattering media" *Physical Review E* **68** 031908 (8 pages) (2003).

III Ilkka Nissilä, Tommi Noponen, Jenni Heino, Timo Kajava, and Toivo Katila "Diffuse optical imaging" in James Lin (ed.), *Advances in Electromagnetic Fields in Living Systems* **4** 77-130, Springer Science (2005, in press).

IV Jenni Heino, Erkki Somersalo, and Simon Arridge "Simultaneous estimation of optical anisotropy and absorption in medical optical tomography" *Proceedings of IVth International Workshop Computational Problems of Electrical Engineering (Zakopane, Poland)* pp 191-194 (2002).

V Jenni Heino and Erkki Somersalo "A modelling error approach for the estimation of optical absorption in the presence of anisotropies" *Physics in Medicine and Biology* **49** 4785-4798 (2004).

VI Jenni Heino, Erkki Somersalo, and Jari Kaipio "Compensation of geometric mismodelling by anisotropies in optical tomography" *Optics Express* **13** 296-308 (2005).

List of abbreviations

The most important abbreviations used in the overview are listed below.

OT	Optical tomography
TPSF	Temporal point spread function
RTE	Radiative transfer equation
PDE	Partial differential equation
DE	Diffusion equation
MC	Monte Carlo
FE	Finite element
FD	Finite difference
MRI	Magnetic resonance imaging
CFS	Cerebrospinal fluid
DT-MRI	Diffusion tensor magnetic resonance imaging
MR	Magnetic resonance
DA	Diffusion approximation
DBC	Dirichlet boundary condition
RBC	Robin boundary condition
BE	Boundary element
EIT	Electrical impedance tomography
MAP	Maximum a posteriori
CM	Conditional mean
ML	Maximum likelihood
MCMC	Markov chain Monte Carlo

1 Introduction

Optical tomography (OT) is a relatively novel modality for non-invasive medical imaging using near-infrared or visible red light. The basic idea in optical tomography is to guide light into the tissue at certain source locations, and collect the transmitted light at a set of measurement locations. The goal is to reconstruct the spatial distribution of the optical parameters of the domain being imaged based on the properties of the measured light. Generally, the parameters of interest are the optical absorption and scattering coefficients of the tissue. These parameters are related to certain physiological quantities, such as the blood volume or concentration of haemoglobin. Using several different wavelengths of light to probe the tissue, it is possible to retrieve information on, e.g., the concentrations of different absorbers such as oxygenated and deoxygenated haemoglobin.

In most tissue types, light propagation is characterised by strong scattering. When constructing models for light propagation in tissue, the scattering is usually assumed to be isotropic, i.e, the probability of scattering into a certain direction is assumed to depend only on the relative angle between the incident and scattered light. Within this assumption, light propagation in OT is commonly modelled using the isotropic diffusion equation. For most tissue types, the assumption of isotropy is a good approximation. However, in some biological tissues with specific type of structures the assumption of isotropy may not hold. Then, light propagation becomes anisotropic, i.e., the probability for the scattering depends on the absolute direction of the incident light.

This thesis is concerned with anisotropic light propagation in the context of optical tomography. The research on this subject is relatively new, and questions related to, e.g., the significance of the anisotropy from the point of view of tomographic applications still need to be investigated. The approach taken in this thesis is computational rather than experimental, and all in all the work should be taken as a conceptual demonstration of the novel methods.

One of the aims of this thesis was to develop light propagation models for the anisotropic case. Successively, another point of focus was the inverse problem of OT assuming that the medium imaged is at least partly anisotropic. This kind of situation raises several questions related to how the anisotropies are treated during the estimation. Adding anisotropy into the model increases the number of parameters in the model. However, it is likely that the background anisotropy is not accurately known, or that no specific prior information is available. The recovery of all the parameters in the anisotropic model is likely to be unsuccessful due to the ill-posedness of the inverse problem. One of the main emphasis in this thesis is on the development of methods that help us to retrieve the estimates of the sought quantities even when the prior information on the background anisotropy is very limited.

This thesis is organized in the following way. Section 2 presents some background on optical tomography and optical anisotropies from the point of view of optical tomography. Section 3 continues by presenting light propagation models for anisotropic media together with the numerical solution. Section 4 is concerned with the inverse problem in the presence of anisotropies. The inverse problem is defined, solution methods presented and the most important results of the thesis reviewed. Section 5 summarizes the work and discusses its significance and some future aspects.

2 Background

2.1 On optical tomography

In optical tomography both implementing the measurements and creating the image of the desired quantity are challenging tasks. Different measurement techniques used in OT can be roughly classified into three categories: the continuous wave, the time domain, and the frequency domain techniques. Continuous wave systems measure the continuous intensity of the detected light. However, especially when both scattering and absorption images are being resolved, time or frequency domain techniques are often used in order to have more information for the reconstruction. In time domain systems, a short picosecond laser pulse is used as the probing signal incident on the tissue, and the temporal behaviour, the so-called temporal point spread function (TPSF) of the transmitted pulse is recorded [1–3]. In frequency domain systems, the optical power of the light source is modulated using a radiofrequency signal, and the amplitude and the phase of the transmitted signal relative to the source are measured [4, 5]. More detailed information on the measurement systems may also be found in Publication III. Generally in OT, the source intensities used are relatively low and the light is strongly attenuated in tissue; hence the measured signals are extremely weak, which poses severe requirements on the measurement system in order to obtain data of reasonable quality. Issues related to, e.g., stability of the light source and electronics, radiofrequency shielding, dynamic range and optode to patient interface may deteriorate the signal and therefore require careful planning [4, Publication III].

The high scattering in most tissue types renders light propagation a diffusion-type process, where photons migrate following complicated paths before being absorbed or escaping through the boundary. Optical tomography is a so-called diffuse imaging modality, where the inverse problem of reconstructing the internal parameter distribution is typically an ill-posed problem requiring sophisticated modelling and reconstruction methods.

A generally used starting point to model light propagation in highly heterogeneous media such as most biological tissues is the radiative transfer equation (RTE). As an integro-differential equation, it is, however, rather tedious to solve, and hence its partial differential equation (PDE) approximations are commonly employed. Nowadays, it has become an almost standard way in OT to model light propagation using the diffusion equation (DE), which can be derived as a special case of the first order spherical harmonics approximation to the RTE. Due to the heterogeneous optical structure of many body parts being imaged, numerical solutions to the forward model equations often need to be used. The most commonly used techniques are the Monte Carlo (MC) simulation implemented based on the RTE, and the finite element (FE) or finite difference (FD) methods to solve the DE. MC simulations

can provide a more accurate solution, but to obtain sufficient statistics, the computation times are often extremely long. The FE or FD solutions to the DE are faster and more commonly used for image reconstruction, whereas MC can be used, e.g., to investigate light propagation in certain tissue structures and to validate other solutions. In some cases, analytical solutions to the PDEs are also used [6–8].

A popular approach for image reconstruction in OT is to formulate the reconstruction problem as a minimization of an objective function of the residual of the measured and model-predicted data with respect to the optical parameter values in the model. Due to the ill-posedness of the problem, a regularizing penalty term on the solution generally needs to be included in the objective function. The computations, especially in 3D, are generally heavy due to the large number of parameters in the discretized model. Various other methods for imaging have also been presented, including perturbation approaches with analytical solutions [8], backprojection and backpropagation algorithms [9–11], linear methods [12], and others [13–15]. The diffuse propagation of light and measurement noise make the spatial resolution attainable with OT inherently poorer than what can be obtained using anatomical medical imaging modalities such as magnetic resonance imaging (MRI) or computed tomography.

Promising clinical applications of optical imaging include imaging of the brain [16,17] to detect and locate hematomas and problems in blood perfusion and oxygenation in newborn babies, brain activation imaging, and imaging of the breast for breast cancer screening. In brain imaging, tomographic imaging is possible with premature infants because of the smaller physical dimensions of the head and thinner skull. During recent years, the first fully three-dimensional reconstructions of the neonatal head have been published [18, 19]. Topographic brain activation imaging to study the hemodynamic changes in response to a stimulus have been performed with both adults [20–22] and infants [23–26]. Optical mammography is a potential application that has received wide interest. The cancerous tissue may have different metabolism and especially the absorption properties of cancerous tissue may differ from those of normal breast tissue. First 3D reconstructions of the breast and clinical studies on breast cancer detection have been presented recently [27–29]. Yet another application of OT is studying the oxidative metabolism of muscles. Spatial information on oxidative metabolism in skeletal muscles during rest and exercise can be retrieved using topographic or tomographic methods [30, 31]. More information on the applications of optical tomography may also be found in Publication III and references therein.

Optical tomography complements existing imaging modalities, and it has a few important advantages compared to some existing techniques. The method does not use ionizing radiation, it is noninvasive and harmless to the patient. The measurement devices can in many cases be made relatively inexpensive and portable. Hence the technique could be used, e.g., for bedside monitoring or noninvasive breast can-

cer screening. Optical imaging can also be used simultaneously with other imaging modalities, as light does not affect low-frequency electromagnetic radiation.

The potential advantages offered by OT on one side, and the great challenges posed by it, on the other side, have made OT a subject of intensive research over the last two decades. One direction has been the development of more refined light propagation models and novel reconstruction methods in order to improve the estimates of the optical parameter distributions. The isotropic diffusion equation that is conventionally used to model light propagation in OT may not always be accurate enough or, in some cases, even useful. A good example of this are the void-like regions, the most important of which when OT is concerned is the cerebrospinal fluid (CSF) in the head. In such clear regions the diffusion equation fails to model the light propagation, and more suitable modelling approaches need to be employed [32–35]. Some other, perhaps less dramatic examples include, e.g., the proximity of sources, where more faithful light propagation models have been constructed by hybrid models that combine the DE in regions far away from the sources with the RTE [36] or MC simulation [37] close to the sources. Also, it has been suggested that the third order approximation (the so called P3 approximation) to the RTE may be useful when highly absorbing or void-like regions are present [38]. Yet another case where the isotropic diffusion equation may not be sufficient is when light propagation depends on absolute direction, i.e., light propagation is anisotropic.

2.2 Optical anisotropies

Generally in optical tomography, light propagation is assumed to be isotropic, i.e., in the macroscopic scale light propagates equally in all directions, assuming that any initial direction is lost by multiple scatterings and disregarding the effect of spatially variant optical properties. In some cases, however, light may have a preferential direction of propagation, and the assumption of isotropy does not hold.

Biological tissues in which anisotropic light propagation may be observed commonly have some structures such as fibres or tubules. Such structural anisotropic characteristics may be observed also in processes other than light propagation, e.g., in the diffusion of water [39, 40] or electrical conductivity [41, 42]. Accurate light propagation models that take also anisotropic characteristics into account may be useful, e.g., in therapeutic and diagnostic applications of light in medicine. In these contexts, light propagation in some tissues that potentially exhibit anisotropic properties has been experimentally explored. In [43], light propagation in chicken breast tissue was measured and found to depend on the relative orientation of the muscle fibers. Similar results have been obtained also for dentin [44], where light propagation depends on the orientation of the tubules, and for skin [45], where the collagen fibres give rise to anisotropic light propagation. In [45], the direction-dependent light propagation in a medium with aligned fibruous or tubular structures was also shown by Monte

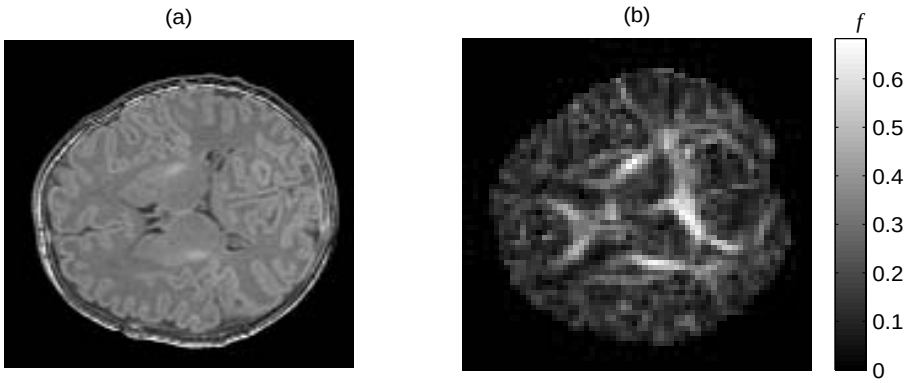

Figure 1: *(a) An anatomical MR image slice from an infant head. (b) A fractional anisotropy f image based on MR-DTI data from an infant head. The fractional anisotropy f was calculated from* $f = (3/2)^{1/2}((\lambda_1 - \lambda)^2 + (\lambda_2 - \lambda)^2 + (\lambda_3 - \lambda)^2)^{1/2}/(\lambda_1^2 + \lambda_2^2 + \lambda_3^2)^{1/2}$*, where* λ_1*,* λ_2 *and* λ_3 *are the eigenvalues that correspond to the eigenvectors of the diffusion tensor and* $\lambda = (\lambda_1 + \lambda_2 + \lambda_3)/3$*.*

Carlo simulations.

Similar tubular structures may also be found in the white matter of the brain, where it is known from diffusion tensor magnetic resonance imaging (MR-DTI) [39, 46, 47] that the anisotropic effects in the diffusion of water are connected to the orientation of the axon bundles. Hence, even though it has not been experimentally verified according to our knowledge, there is good reason to believe that light propagation in the white matter of the brain is anisotropic. How strong this anisotropy may be, is a question still unanswered, as well as the significance of the phenomenon in the context of OT. In Ref. [48], a Monte Carlo simulation study for light propagation in a topographic measurement setup at one side of the head was conducted. In this study, magnetic resonance (MR) images for the anatomical structure and MR-DTI data for tissue anisotropy of an adult head were used, and the strength of the anisotropy in light propagation was assumed to be comparable to that of water diffusion in the MR-DTI data. Simulations omitting and including the anisotropic effects were compared. For the adult head, the results, though some difference between the isotropic and anisotropic cases could be seen, did not demonstrate statistically significant differences. An attempt to model the head of an infant was then done by scaling down the model of the adult head. In this case, clear and statistically significant differences were observed for some detector positions. The infant model is of course a crude approximation due to differences, e.g., in the anatomical structure and the state of myelinisation of the white matter axon bundles between the adult and infant head. However, in a tomographic measurement setup it is likely that the effects due to the white matter of the brain are more pronounced, and the anisotropic effect may be more significant. Indeed, preliminary results [49]

from MC simulation using MR and MR-DTI data of an infant head indicate that for certain source and detector positions in the transmission geometry the effect of anisotropy on the amplitude is clearly significant, up to approximately 50 percent. Figure 1 displays anatomical MR and fractional anisotropy slices from the infant head MR and MR-DTI data that was used in the simulation.

In connection of medical optical tomography and imaging, research on anisotropic light propagation is a relatively new topic. The full radiative transfer model is capable of modelling anisotropic behaviour, but for OT, numerical solutions to the RTE are often computationally too demanding. For now, most published results concentrate on the forward problem. Different approaches taken for modelling anisotropic light propagation include Monte Carlo techniques [45, 48, Publication II], the so called *random walk* method [50–52], and a PDE-based approach using an anisotropic diffusion equation [53, 54, Publications I,II,IV-VI]. Monte Carlo techniques have been applied, at least, to construct a model for light propagation in the head and to compare the results from MC simulations with those obtained using the diffusion equation. The anisotropic random walk method was first introduced in [50], and generalized further in [51]. Recently, the research group at University College London has built a solid anisotropic phantom using an epoxy resin cube containing parallel holes filled with paraffin wax. The effective scattering coefficient for the wax was lower than that of the epoxy, hence enabling the light to propagate better in direction parallel to the paraffin wax rods. Measurements on this phantom were fitted to the predictions of the anisotropic random walk model in [52].

The partial differential equation based approach utilizing the diffusion equation is particularly suitable when the inverse problem of determining the optical properties is considered, as the diffusion equation can be solved numerically relatively quickly for inhomogeneous media. First approaches to solve the inverse problem in the presence of anisotropies may be found in Publications I, IV, V, and [53]. Methods developed to treat anisotropies may also become useful to handle other problems in OT such as inaccurate modelling of the geometry, as demonstrated in Publication VI.

3 Forward problem in the presence of anisotropies

3.1 Models for light propagation

3.1.1 Radiative Transfer Equation

The Maxwell equations describe the propagation of light in a medium. In the case of near-infrared radiation in biological tissue, however, the characteristic distances in the medium are so large compared to the wavelength of the light, that exact light propagation models become impractical. A generally used model for light propagation in turbid media is the radiative transfer equation [55, 56]. For a time-dependent problem it is written

$$\begin{aligned}\frac{1}{c}\frac{\partial}{\partial t}L(\mathbf{r},\hat{\mathbf{s}},t) + \hat{\mathbf{s}}\cdot\nabla L(\mathbf{r},\hat{\mathbf{s}},t) + \mu_{\mathrm{a}}(\mathbf{r})L(\mathbf{r},\hat{\mathbf{s}},t) + \mu_{\mathrm{s}}(\mathbf{r})L(\mathbf{r},\hat{\mathbf{s}},t)& \\ = \mu_{\mathrm{s}}(\mathbf{r})\int_{S^{m-1}}\Theta(\hat{\mathbf{s}},\hat{\mathbf{s}}\,',\mathbf{r})L(\mathbf{r},\hat{\mathbf{s}}\,',t)\,\mathrm{d}\hat{\mathbf{s}}\,' + q(\mathbf{r},\hat{\mathbf{s}},t),& \qquad (1)\end{aligned}$$

where $L(\mathbf{r},\hat{\mathbf{s}},t)$ is the *radiance* in direction $\hat{\mathbf{s}}$ at time t at point $\mathbf{r}\in\mathbb{R}^m$, $m=2,3$, c is the speed of light in the medium, $\mu_{\mathrm{a}}(\mathbf{r})$ and $\mu_{\mathrm{s}}(\mathbf{r})$ the spatial distributions of the absorption and scattering coefficients, respectively, and $q(\mathbf{r},\hat{\mathbf{s}},t)$ the spatial and angular distribution of the source. The term $\Theta(\hat{\mathbf{s}},\hat{\mathbf{s}}\,',\mathbf{r})$ is the so-called *scattering phase function* which represents the probability of scattering from direction $\hat{\mathbf{s}}\,'$ into the direction $\hat{\mathbf{s}}$.

The RTE is a balance equation for the radiance L, which can be defined so that the energy transfer in the infinitesimal angle $d\hat{\mathbf{s}}$ in direction $\hat{\mathbf{s}}$ at time t through an infinitesimal area da is given by

$$L(\mathbf{r},\hat{\mathbf{s}},t)\hat{\mathbf{s}}\cdot\hat{\mathbf{n}}\,da\,d\hat{\mathbf{s}}, \qquad (2)$$

where $\hat{\mathbf{n}}$ is the normal to the surface da. The physical interpretation of the terms in RTE is perhaps more obvious if we consider integration over an infinitesimal volume dV. The first term in the left-hand-side is the change in the radiance at time t in the infinitesimal volume dV at point $\mathbf{r}$ in direction $\hat{\mathbf{s}}$. The second term represents the loss of photons through the surfaces of the volume dV, the third the loss due the absorption, and the fourth the loss due to scattering from direction $\hat{\mathbf{s}}$ into other directions. On the right-hand-side, the first term comprises the gain due to scattering from all other directions into the direction $\hat{\mathbf{s}}$ and the second the gain through the light source q. Shifting all terms except the first one to the right-hand-side of the equation, we see that the change in the radiance is obtained simply as a superposition of the rest of the terms representing the loss and gain of the photons.

The scattering phase function is a non-negative function satisfying

$$\int_{S^{m-1}}\Theta(\hat{\mathbf{s}},\hat{\mathbf{s}}\,')\,\mathrm{d}\hat{\mathbf{s}} = 1 \qquad \forall\,\hat{\mathbf{s}}\,'\in S^{m-1} \qquad (3)$$

(probability of scattering over the sphere is unity for all directions of incoming light) and $\Theta(\hat{\mathbf{s}}, \hat{\mathbf{s}}') = \Theta(-\hat{\mathbf{s}}', -\hat{\mathbf{s}})$ (reciprocity of light propagation).

In the special case where the scattering phase function only depends on the relative angle between the incoming and outgoing radiation, i.e.,

$$\Theta(\hat{\mathbf{s}}, \hat{\mathbf{s}}', \mathbf{r}) = \Theta_{\text{iso}}(\hat{\mathbf{s}} \cdot \hat{\mathbf{s}}', \mathbf{r}), \tag{4}$$

scattering is called isotropic. Finally, let us define the energy current density $\mathbf{J}$

$$\mathbf{J}(\mathbf{r}, t) = \int_{S^{m-1}} L(\mathbf{r}, \hat{\mathbf{s}}, t)\hat{\mathbf{s}} \, \mathrm{d}\hat{\mathbf{s}} \tag{5}$$

and the energy fluence Φ

$$\Phi(\mathbf{r}, t) = \int_{S^{m-1}} L(\mathbf{r}, \hat{\mathbf{s}}, t) \, \mathrm{d}\hat{\mathbf{s}}. \tag{6}$$

Numerical solutions to the RTE often lead to a computational problem far too large from the point of view of solving the inverse problem. Therefore, simplifications to the RTE are generally used. The most frequently used approximation, the isotropic diffusion approximation (DA), is well established in the literature. For the anisotropic case, the equivalent model is the anisotropic diffusion equation, which is also the approach taken in this thesis.

3.1.2 Diffusion approximation

Isotropic case

A standard way to derive the diffusion approximation from the RTE is to expand the radiance $L(\mathbf{r}, \hat{\mathbf{s}}, t)$ and the source term $q(\mathbf{r}, \hat{\mathbf{s}}, t)$ in the RTE into series using the spherical harmonics [56–58]

$$L(\mathbf{r}, \hat{\mathbf{s}}, t) = \sum_{l=0}^{\infty} \sum_{m=-l}^{l} \sqrt{\frac{2l+1}{4\pi}} L_{lm}(\mathbf{r}, t) Y_{lm}(\hat{\mathbf{s}}), \tag{7}$$

$$q(\mathbf{r}, \hat{\mathbf{s}}, t) = \sum_{l=0}^{\infty} \sum_{m=-l}^{l} \sqrt{\frac{2l+1}{4\pi}} q_{lm}(\mathbf{r}, t) Y_{lm}(\hat{\mathbf{s}}). \tag{8}$$

Also, in the isotropic case the assumption of isotropic scattering, i.e., $\Theta(\hat{\mathbf{s}}, \hat{\mathbf{s}}', \mathbf{r}) = \Theta_{\text{iso}}(\hat{\mathbf{s}} \cdot \hat{\mathbf{s}}', \mathbf{r})$, is made. The scattering phase function is then expanded into series using Legendre polynomials, which, using the addition theorem, can be written

$$\Theta_{\text{iso}}(\hat{\mathbf{s}} \cdot \hat{\mathbf{s}}', \mathbf{r}) = \sum_{l=0}^{\infty} \sum_{m=-l}^{l} \Theta_{\text{iso},l}(\mathbf{r}) Y_{lm}^{*}(\hat{\mathbf{s}}') Y_{lm}(\hat{\mathbf{s}}). \tag{9}$$

An often used form for the isotropic scattering phase function is the Henyey-Greenstein function (in 3D) [59, 60]

$$\Theta_{\mathrm{HG}}(\hat{\mathbf{s}} \cdot \hat{\mathbf{s}}\,') = \frac{1}{4\pi} \frac{1 - g^2}{(1 + g^2 - 2g\hat{\mathbf{s}} \cdot \hat{\mathbf{s}}\,')^{3/2}}\,, \tag{10}$$

which is a heuristic function that has been used to model, e.g., scattering from blood cells and clouds. Above, g denotes $\Theta_{\mathrm{iso},1}$, the average of the cosine of the scattering angle

$$g = \Theta_{\mathrm{iso},1} = \int_{S^2} \Theta_{\mathrm{iso}}(\hat{\mathbf{s}} \cdot \hat{\mathbf{s}}\,')(\hat{\mathbf{s}} \cdot \hat{\mathbf{s}}\,')\,\mathrm{d}\hat{\mathbf{s}}\,'. \tag{11}$$

In the sequel, we refer to the parameter g as the *bias factor*.

The so-called P_N approximation to the RTE is obtained by inserting the expansions (7), (8) and (9) into the RTE (1) and truncating the series at $l = N$. After some lengthy calculations, this leads to a set of $(N + 1)^2$ coupled equations.

The diffusion approximation is derived from the P_1 approximation. Truncating the series at $l = 1$ leads to a pair of coupled equations

$$\left(\frac{1}{c}\frac{\partial}{\partial t} + \mu_{\mathrm{a}}(\mathbf{r})\right) \Phi(\mathbf{r}, t) + \nabla \mathbf{J}(\mathbf{r}, t) = q_0(\mathbf{r}, t) \tag{12}$$

$$\left(\frac{1}{c}\frac{\partial}{\partial t} + \mu_{\mathrm{a}}(\mathbf{r}) + (1 - g)\mu_{\mathrm{s}}(\mathbf{r})\right) \mathbf{J}(\mathbf{r}, t) + \frac{1}{3}\nabla\Phi(\mathbf{r}, t) = \mathbf{q}_1(\mathbf{r}, t), \tag{13}$$

where Φ and $\mathbf{J}$ are defined in Eqs. (6) and (5), and q_0 and $\mathbf{q}_1$ are given by

$$q_0(\mathbf{r}, t) = \int_{S^{m-1}} q(\mathbf{r}, \hat{\mathbf{s}}, t)\,\mathrm{d}\hat{\mathbf{s}}, \tag{14}$$

$$\mathbf{q}_1(\mathbf{r}, t) = \int_{S^{m-1}} \hat{\mathbf{s}} q(\mathbf{r}, \hat{\mathbf{s}}, t)\,\mathrm{d}\hat{\mathbf{s}}. \tag{15}$$

In the case of P_1 approximation, this set can also be derived without explicit expansion of the phase function $\Theta_{\mathrm{iso}}(\hat{\mathbf{s}} \cdot \hat{\mathbf{s}}\,', \mathbf{r})$. For details, see, e.g., [56, 60].

The P_1 approximation (12)-(13) can be reduced to a single equation by making the assumptions that $\mathbf{q}_1$ vanishes and $\frac{\partial \mathbf{J}}{\partial t}$ is negligible. Equation (13) then simplifies into Fick's law

$$\mathbf{J} = -\kappa_0 \nabla \Phi, \tag{16}$$

where the *diffusion coefficient* is defined by

$$\kappa_0 = \frac{1}{m(\mu_{\mathrm{a}} + \mu_{\mathrm{s}}')} \tag{17}$$

and $\mu_{\mathrm{s}}' = (1 - g)\mu_{\mathrm{s}}$ is the *reduced scattering coefficient*. Substituting the Fick's law into Eq. (12), we arrive at the isotropic diffusion equation

$$\frac{1}{c}\frac{\partial}{\partial t}\Phi(\mathbf{r}, t) - \nabla \cdot \kappa_0(\mathbf{r})\nabla\Phi(\mathbf{r}, t) + \mu_{\mathrm{a}}(\mathbf{r})\Phi(\mathbf{r}, t) = q_0(\mathbf{r}, t). \tag{18}$$

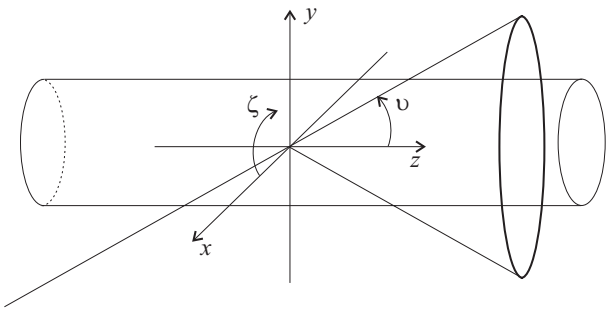

Figure 2: *A schematic representation of the anisotropic scattering model. The component of light parallel to the axis of the cylinder (z–axis) is preserved in the scattering, whereas the perpendicular component obeys the 2D Henyey-Greenstein function. The cone represents the possible scattering directions. When $g_\perp = 0$, i.e., scattering is uniform in the xy–plane, the scattering probability is distributed evenly on the cone.*

The assumption that $\mathbf{q}_1 = 0$ means that an isotropic source term is assumed. The second assumption, $\frac{\partial \mathbf{J}}{\partial t}$ is negligible, can be justified for modulation frequencies less than $\sim$1 GHz for the case $\mu_\mathrm{a} << \mu_\mathrm{s}'$. For more details, see, e.g., Publication III and [57, 58, 61, 62]. The diffusion model is widely used and considered valid for most cases. Some important exceptions are, e.g., the proximity of light sources and non-scattering regions. For more discussion and results, see, e.g., Publication III, [57, 58, 61–69].

Anisotropic case

For the anisotropic case, a similar derivation using the spherical harmonics can be conducted. The question then arises, though, as to what kind of function to use for the scattering phase function Θ. One possible derivation is presented in Publication II, where a phase function is constructed by considering an infinite cylinder oriented in the direction of the z-axis. The direction of scatter is assumed unchanged in the z-direction, whereas in the xy-plane isotropic scattering is assumed. A model for the phase function is then written as

$$\Theta_\mathrm{aniso}(\hat{\mathbf{s}}, \hat{\mathbf{s}}\,') = \Theta(\upsilon, \upsilon', \zeta, \zeta'; g_\perp) = \delta(\cos\upsilon - \cos\upsilon')\Theta_\mathrm{HG,2}(\zeta, \zeta'; g_\perp), \qquad (19)$$

where $\Theta_\mathrm{HG,2}$ is the two-dimensional analog of the Henyey-Greenstein function

$$\Theta_\mathrm{HG,2}(\zeta, \zeta'; g_\perp) = \frac{1}{2\pi}\frac{1 - g_\perp^2}{(1 + g_\perp^2 - 2g_\perp\cos(\zeta - \zeta'))}\,, \qquad (20)$$

and $g_\perp$ represents the bias factor for scattering in the xy-plane. The anisotropic scattering model is illustrated in Fig. 2.

Expanding the phase function (19) into spherical harmonics and performing the standard derivation results into the anisotropic diffusion equation (for more details, see Publication II)

$$\frac{1}{c}\frac{\partial}{\partial t}\Phi(\mathbf{r},t) - \nabla\cdot\kappa(\mathbf{r})\nabla\Phi(\mathbf{r},t) + \mu_{\mathrm{a}}(\mathbf{r})\Phi(\mathbf{r},t) = q_0(\mathbf{r},t). \tag{21}$$

Above, the *diffusion tensor* κ is given by

$$\kappa = \frac{1}{3}\left(\mu_{\mathrm{a}}I + (I - S_1)\mu_{\mathrm{s}}\right)^{-1}, \tag{22}$$

where I denotes the identity matrix and

$$S_1 = \begin{pmatrix} g_\perp & 0 & 0 \\ 0 & g_\perp & 0 \\ 0 & 0 & 1 \end{pmatrix} \tag{23}$$

To generalize the representation of the diffusion tensor, we imagine a mixture of oriented fibres and isotropic scatterers with fractions f and $(1-f)$, respectively, and assume that the isotropic scatterers have a bias factor g_0. The diffusion tensor is then obtained using

$$S_1 = \begin{pmatrix} fg_\perp + (1-f)g_0 & 0 & 0 \\ 0 & fg_\perp + (1-f)g_0 & 0 \\ 0 & 0 & f + (1-f)g_0 \end{pmatrix} \tag{24}$$

Furthermore, the diffusion tensor along some other direction is obtained by rotating the original diffusion tensor

$$\kappa \to R\kappa R^T, \tag{25}$$

where $R \in \mathbb{R}^{m\times m}$ is a rotation matrix.

A second possibility to derive the anisotropic diffusion approximation is presented in Publication I, where the spherical harmonics are not used explicitly. Instead, an orthogonal projection operator is defined, and the derivation is conducted by calculating the projection into the subspace spanned by the zeroth and the first order polynomials in S^{m-1}. This results into an anisotropic diffusion equation of the form (21) with the diffusion coefficient defined by

$$\kappa = \frac{1}{m}((\mu_{\mathrm{a}}I + (I-B)\mu_{\mathrm{s}})^{-1} \in \mathbb{R}^{m\times m}, \tag{26}$$

where I is the identity matrix and $B = B(\mathbf{r}) \in \mathbb{R}^{m\times m}$ is a matrix with elements

$$B_{i,j}(\mathbf{r}) = \frac{m}{|S^{m-1}|}\int_{S^{m-1}}\int_{S^{m-1}} s_i s_j' \Theta(\hat{\mathbf{s}}, \hat{\mathbf{s}}\,', \mathbf{r})\,\mathrm{d}\hat{\mathbf{s}}\,\mathrm{d}\hat{\mathbf{s}}\,'. \tag{27}$$

Above, s_i and s'_j represent the ith and the jth components of $\hat{\mathbf{s}}$ and $\hat{\mathbf{s}}'$, respectively. Yet another possibility to derive the anisotropic DA with again a slightly different definition for the diffusion tensor is presented in [48].

Frequency domain

In this work, the diffusion equation is solved in the frequency domain. Assume a point source at $\mathbf{r} = \mathbf{r}_s$ modulated with an angular frequency ω,

$$q_0(\mathbf{r}, t) = \delta(\mathbf{r} - \mathbf{r}_s)(Q_0 + Se^{-i\omega t}), \tag{28}$$

where Q_0 is the dc amplitude and S the modulation amplitude of the source. The frequency domain analog of the diffusion equation (21) is obtained by taking the Fourier transform of (21):

$$-\frac{i\omega}{c}\Phi(\mathbf{r};\omega) - \nabla \cdot \kappa(\mathbf{r})\nabla\Phi(\mathbf{r};\omega) + \mu_{\mathrm{a}}(\mathbf{r})\Phi(\mathbf{r};\omega) = q_0(\mathbf{r};\omega), \tag{29}$$

where $\Phi(\mathbf{r};\omega)$ is the complex fluence arising from the intensity modulated part $q_0(\mathbf{r};\omega)$ of the source term.

3.1.3 Boundary and source conditions

In the literature, there are a few boundary and source conditions that have been adopted for the diffusion equation in optical imaging [54, 56, 57, 60, 61, 65, 67, 68, Publication II]. The simplest boundary condition is the Dirichlet boundary condition (DBC), where the fluence on the boundary is set to zero. Another possibility is to use the so-called extrapolated boundary condition, where a virtual boundary is placed at a certain distance from the real boundary, and the Dirichlet condition is applied at this extrapolated boundary. Perhaps the most popular boundary condition, and the approach that we also adopt in this thesis, is the so-called Robin boundary condition (RBC), which can be derived from the condition that the total inward directed current at each point on the boundary is zero. Without refractive index mismatch, the RBC is written

$$\Phi(\mathbf{r}, t) + \frac{1}{2\gamma}\hat{\mathbf{n}} \cdot \kappa(\mathbf{r})\nabla\Phi(\mathbf{r}, t) = 0 \qquad \forall \mathbf{r} \in \partial\Omega, \tag{30}$$

where $\hat{\mathbf{n}}$ is the outward unit normal vector to the boundary $\partial\Omega$, and the constant $\gamma = \gamma_m$ depends on the dimension m and has values $\gamma_2 = 1/\pi$, $\gamma_3 = 1/4$.

To model the light source, two different approaches are commonly employed. One possibility is to use a diffuse source on the boundary. The source is represented as an inward-directed current over the illuminated area on the boundary. The diffuse source can be incorporated directly into the DBC and RBC. The second approach,

which is what we use in this thesis, is to treat the light source as a collimated pencil beam incident on the boundary. A usual way to model the pencil beam is to represent it as an isotropic point source located at a depth $1/\mu_{\mathrm{s}}'$ under the surface of the body.

On the boundary, the measurement data consists of the outward boundary flux $\Phi_{\mathrm{out}} = -\hat{n} \cdot \kappa \nabla \Phi$ at the measurement locations $\mathbf{r}_{\mathrm{meas}} \in \partial\Omega$. For the purpose of image reconstruction, one or more measurement types are usually derived from the outward boundary flux [67, 70–72]. In this thesis, the numerical work is done in the frequency domain, and for the measurement quantities we use the logarithm of the amplitude $\ln A = \ln |\Phi_{\mathrm{out}}|$ and the phase angle $\varphi = \arg \Phi_{\mathrm{out}}$ of the complex boundary flux.

3.2 Numerical solution using finite elements

Perhaps the most frequently utilised approaches for the numerical solution of partial differential equations in optical tomography are the finite difference (FD) [63, 73–77] and the finite element (FE) [13, 33, 38, 67, 68, 78–93] methods. Of these, the finite element method is more widely used due to its flexibility in modelling physiological tissue shapes and inhomogeneous material parameter distributions. Most of the numerical simulations in this work are based on the FE method.

The implementation of the finite element solution to the diffusion equation starts by the variational formulation. Assume that we want to solve the diffusion equation in a body $\Omega \subset \mathbb{R}^m$. By multiplying the DA (29) by a test function ψ, integrating by parts over Ω, and including the RBC (30), we get the weak formulation of the problem: *Find* Φ *such that*

$$\int_\Omega \nabla\psi \cdot \kappa \nabla\Phi d\mathbf{r} + \int_\Omega (\mu_{\mathrm{a}} - \frac{i\omega}{c})\psi\Phi d\mathbf{r} + \int_{\partial\Omega} 2\gamma\psi\Phi dS = q_0\psi(\mathbf{r}_s) \tag{31}$$

$\forall\psi \in H^1(\Omega)$, where $H^1(\Omega)$ is a predefined function space (Sobolev space) for the test functions. In the above form, a point source at $\mathbf{r} = \mathbf{r}_s$ is assumed.

The finite element approximation consists of dividing the domain Ω into a set of finite elements, and approximating the solution by nodal-based basis functions

$$\Phi(\mathbf{r}) \approx \Phi^h(\mathbf{r}) = \sum_{j=1}^{N_{\mathrm{n}}} \alpha_j \psi_j(\mathbf{r}), \tag{32}$$

where N_{n} is the number of nodes in the finite element mesh. By requiring that Φ^h satisfies Eq. (31) $\forall\psi_j \in \{\psi_i\}_1^{N_{\mathrm{n}}}$ we arrive at the matrix equation $A\alpha = \beta$, where A is the $N_{\mathrm{n}} \times N_{\mathrm{n}}$ symmetric matrix with elements

$$A_{j,\ell} = \int_\Omega \nabla\psi_j \cdot \kappa \nabla\psi_\ell d\mathbf{r} + \int_\Omega (\mu_{\mathrm{a}} - \frac{i\omega}{c})\psi_j\psi_\ell d\mathbf{r} + \int_{\partial\Omega} 2\gamma\psi_j\psi_\ell dS, \tag{33}$$

and β is a $N_\mathrm{n} \times 1$ vector $\beta_j = q_0 \psi_j(\mathbf{r}_s)$.

The numerical simulations in this work are conducted in two-dimensional space. In 2D, we write the diffusion coefficient $\kappa \in \mathbb{R}^2$

$$\kappa(\mathbf{r}) = U(\mathbf{r})\mathrm{diag}(\lambda_1(\mathbf{r}), \lambda_2(\mathbf{r}))U(\mathbf{r})^\mathrm{T}, \tag{34}$$

where

$$\lambda_j(\mathbf{r}) = \frac{1}{2(\mu_\mathrm{a}(\mathbf{r}) + (1 - b_j(\mathbf{r}))\mu_\mathrm{s}(\mathbf{r}))}, \quad j = 1, 2. \tag{35}$$

The above form is obtained straightforwardly from Eqs. (22)-(25), and in the case of Eqs. (26)-(27) it is obtained from the eigenvalue decomposition of B: $B = U\mathrm{diag}(b_1, b_2)U^\mathrm{T}$. By denoting the angle of the first eigenvector $\bar{a}_1$ in the matrix $U \in \mathbb{R}^2$ by θ, U is written as

$$U(\mathbf{r}) = (\bar{a}_1(\mathbf{r}) \;\; \bar{a}_2(\mathbf{r})) = \begin{pmatrix} \cos\theta(\mathbf{r}) & -\sin\theta(\mathbf{r}) \\ \sin\theta(\mathbf{r}) & \cos\theta(\mathbf{r}) \end{pmatrix}. \tag{36}$$

The angle $\theta(\mathbf{r})$ containing the information on the direction of anisotropy is restricted to the interval $0 \leq \theta(\mathbf{r}) < \pi$.

Apart from the first term, the system matrix A is essentially the same as in an isotropic case. We note that the first term may be written as

$$\int_\Omega \nabla\psi_j \cdot \kappa \nabla\psi_\ell d\mathbf{r} = \int_\Omega \lambda_1(\bar{a}_1 \cdot \nabla\psi_j)(\bar{a}_1 \cdot \nabla\psi_\ell)d\mathbf{r} + \int_\Omega \lambda_2(\bar{a}_2 \cdot \nabla\psi_j)(\bar{a}_2 \cdot \nabla\psi_\ell)d\mathbf{r}. \tag{37}$$

Furthermore, if the strength of the anisotropy is assumed to be constant, i.e., the parameters λ_1 and λ_2 have constant values, these parameters can be taken out from the integrals.

3.3 Comparison of numerical solutions

A common way to test the validity of a simplified computational model, such as the diffusion equation, is to compare the results of the model with Monte Carlo simulations [33,37,65,67,94,95]. In Publication II, we have compared the FE model for the anisotropic frequency domain diffusion equation (29) with Monte Carlo simulations and the boundary element (BE) method [96–98] solution to (29).

The anisotropic Monte Carlo simulation was based on an isotropic time-domain Monte Carlo code [66,99]. The MC code proceeds by successively launching photon packets into the medium and following their propagation until they are completely absorbed or escape through the boundary of the medium. The absorption is modelled by introducing a weight to the photon packet and reducing the weight at each scattering step relative to the probability of absorption. As the photon exits on the

boundary, the weight of the packet is recorded. To model anisotropic media, the anisotropic scattering model described in Fig. 2 and Eqs. (19)–(20) with $g_\perp = 0$, i.e., uniform scattering in the plane perpendicular to the direction of anisotropy, was implemented into the MC code. Anisotropic scattering was assumed to take place with probability f, otherwise an isotropic scattering with uniform probability distribution for the scattering angle was simulated. In order to simulate frequency domain measurements, the phase shift and the complex intensity were calculated based on the pathlength and weight of the photon packets exiting the medium.

To implement the corresponding diffusion model, the anisotropic diffusion equation (29) with the diffusion coefficient defined by Eqs. (22)–(24) was utilised. The diffusion model was solved in 2D using both FE and BE methods. For the details of the implementation of the BE method, see Publication II.

The MC simulation was conducted in a 3D cylinder, and the FE and BE calculations in a disk corresponding to a cross-section of the cylinder. Although the MC simulation was conducted in 3D and the FE and BE models in 2D, the results could be compared by modelling the detectors in 3D by line detectors parallel to the axis of the cylinder. The results of the simulations indicate that the anisotropic effects could be modelled with the diffusion model sufficiently, provided that the anisotropy used is presentable in the diffusion framework. For details of the simulations and results, see Publication II.

4 Solving the inverse problem

4.1 Inverse problem in OT with background anisotropies

A rigorous and commonly adopted approach for solving the inverse problem is to use model-based estimation methods that rely on a forward model of the measurements. The inverse problem then becomes the problem of recovering the relevant parameters of the forward model, and hence the definition of the inverse problem depends on the forward model chosen. Throughout this thesis, we concentrate on the inverse problem of finding the relevant parameters under the diffusion model. In the isotropic case, the inverse problem generally consists of finding the spatial distributions of the absorption and the scattering or the diffusion coefficients based on the boundary data. By defining a non-linear forward operator G, the forward model can be expressed as

$$y = G(p; q), \tag{38}$$

where y is the data predicted by the forward operator, given the internal parameter distribution p and the distribution of sources q. The solution of the inverse problem can then formally be written as

$$p = G^{-1}(y; q). \tag{39}$$

The inverse problem of optical tomography suffers from severe ill-posedness, which, together with the measurement noise and discrepancies between the model and reality in the case of measured data, ensure that solving the inverse problem is often a complicated task. The non-uniqueness of the inverse problem in the isotropic case has been assessed in [100], where the authors showed that the recovery of both the absorption and the diffusion coefficients based on steady-state measurements is a non-unique problem. However, in the case of time/frequency-domain data, uniqueness could in principle be proven at the limit of complete continuous measurements and source distributions and assuming the refractive index to be known. However, in a real world problem with discrete measurements, the unique recovery of the distribution of the absorption and diffusion coefficients is likely to be unfeasible. In practice, simultaneous estimates of both the absorption and the diffusion coefficients are retrieved through imposing some prior knowledge on the solution into the estimation scheme.

In the anisotropic case, however, the situation is even more complicated. Using the anisotropic diffusion equation as the forward model, instead of single scalar diffusion coefficient κ_0, the diffusion is modelled with a tensor κ. The non-uniqueness of the inverse anisotropic conductivity problem in electrical impedance tomography (EIT), which is a similar problem to the inverse anisotropic diffusion problem in OT, has been proven both in 3D and 2D [101, 102]. One source of non-uniqueness are diffeomorphic transformations that leave the boundary intact. Similarly, in OT

the inverse problem of defining the anisotropic diffusion tensor and the absorption coefficient simultaneously suffers from non-uniqueness. Hence an attempt to estimate both the absorption coefficient and the diffusion tensor without essential prior knowledge is very likely to fail.

As mentioned above, to help the estimation in the case of an ill-posed problem, prior information on the unknown parameters is generally used to modify the problem towards a more well-posed one. One way to impose the prior information is to reduce the number of sought parameters by implementing knowledge on, e.g., region boundaries or parameter values. Another way is to introduce a regularizing functional into the objective functional that is minimized in the solution. The regularizing functional may contain penalty terms to regulate, e.g., the norm, the variance, or the smoothness of the solution. However, often it may be that prior information is available, but the nature of the information is such that the essential problem then is on the implementation of this information into the estimation. In those cases, statistical methods may provide a way to implement the prior information. The cost, however, is often that the implementation of the statistical approach leads to methods that are computationally demanding and expensive.

In the case of anisotropies, prior information may be available based on, e.g., anatomical information or information from another imaging modality such as diffusion tensor imaging. However, often specific prior information such as MR-DTI data is not available, or it may be that the prior information at hand is not very accurate or reliable. The kind of prior information one is most likely to have could be suggestive information on the directions of anisotropy, e.g., from the knowledge of the anatomical structure of the muscles or the brain. Even in the case that MR-DTI data is available, drawing elaborate conclusions on the strength of the anisotropy may be unjustified.

The approach taken in this thesis is to assume that we have a parameter of *primary* interest, which we choose to be the absorption coefficient. The rest of the unknown parameters, in this case the parameters defining the diffusion tensor, are mainly seen as parameters of *secondary* interest that compromise the reconstruction of the primary parameter of interest. We do not attempt to determine the diffusion tensor parameters, or at least not all of them, during the estimation, but try to estimate the absorption coefficient and reduce the disturbing effect of the background anisotropy. In addition to the fact that even the recovery of the diffusion tensor alone without adequate prior knowledge may prove to be practically impossible, we justify this choice by considering the potential applications. From the point of view of clinical applications, there are several cases where knowledge on the absorption coefficient alone can be valuable and provide diagnostic information. In tomographic imaging of the infant head, the goal may be to detect and localize hematomas or problems in blood perfusion, which are phenomena that could be monitored using information on the absorption only. In imaging of the muscles, the phenomena of interest are

likewise related to the amount and the oxygenation state of the blood, which are reflected in the absorption coefficient. For completeness let us note that also in breast cancer imaging, though there anisotropies are likely to be of much less significance than in the two previous examples, cancerous tissue has been reported to exhibit from 1.25 to 3 times higher absorption than the normal one [103].

When encountering a situation where background anisotropies are present, the simplest and the most straightforward approach is simply to ignore the anisotropies and use the conventional isotropic model for the inversion. Alternatively, one might assume that enough prior information is available on the background anisotropy to fix certain anisotropy parameter values and enable the reconstruction of the remaining ones. Moving on towards more sophisticated approaches, the next step considered in this thesis is to utilise methods to reduce the degrading effect of the secondary parameters, i.e., anisotropy parameters, on the estimate of the absorption coefficient. The limited prior information on the anisotropies may be implemented into these methods. However, the problem of imposing prior knowledge in the estimation still remains, and more complex priors require sophisticated modelling and computational means that, for the most part, are out of the scope of this thesis.

In the following, we first briefly review some optimization methods used in this thesis. Also, we give a brief outline of the statistical thinking, as the work presented here is related to and has extension in statistical inversion methods. The solution methods to the anisotropic inverse problem used in this thesis are then likewise briefly reviewed, together with a numerical example of some of the methods. For more details and results the reader is referred to Publications I, IV and V. Finally, to demonstrate that the methods developed might be useful also for problems other than anisotropic tissue structures, we present an application, published in Publication VI, of the methods to deal with inaccurately known boundary geometry and optode positions.

4.2 Gauss-Newton and Levenberg-Marquardt algorithms

Assuming additive measurement noise n the observation model adopted in this work is written as

$$y = G(p) + n, \tag{40}$$

where y is a vector containing the measurements, p a vector containing the discretized parameter values, G the model for the noiseless observation and n the vector containing the additive measurement noise. The solution to the inverse problem is often formulated as an optimization problem of minimizing an objective functional involving the difference between the measured and model predicted data. One popular approach is the least squares method (see, e.g., [104–106]), where the

minimization problem is to find p that minimizes the functional

$$F(p) = ||y - G(p)||^2. \tag{41}$$

In practice, to obtain useful estimates, regularization needs to be used. A very commonly used regularization method is the *Tikhonov* regularization (see, e.g. [107]), where the least squares functional is modified by adding a regularizing penalty term. Also, if prior information on the structure of the additive noise is available, the minimization can be done in the weighted least squares sense by scaling the residual with a weight matrix L_w. Including the weighting and the Tikhonov regularization in the generalized form, the objective functional becomes

$$F(p) = ||L_w(y - G(p))||^2 + \alpha f(p), \tag{42}$$

where $\alpha > 0$ is the regularization parameter. Assuming, e.g., that W is a diagonal noise covariance matrix, one possible way to choose the weighting matrix L_w is to set $L_w^T L_w = W^{-1}$. A commonly used form for the functional $f(p)$ is

$$f(p) = ||L(p - p_*)||^2, \tag{43}$$

where L is a regularization matrix and p_* represents a plausible value of p based on prior knowledge.

The *Gauss-Newton* method for the problem (42) can be derived from a sequence of linearizations for the non-linear operator G. If p_k is the current estimate of p, we write the linearization as

$$G(p) \approx G(p_k) + G'(p)|_{p=p_k}(p - p_k) \equiv G(p_k) + J(p - p_k), \tag{44}$$

where J denotes the Jacobian matrix of the non-linear forward model with respect to p at the current estimate $p = p_k$. The minimization proceeds iteratively by minimizing the linearized approximation

$$F(p) \approx \tilde{F}(p) = ||L_w(y - G(p_k) - J(p - p_k))||^2 + \alpha||L(p - p_*)||^2, \tag{45}$$

where we have adopted a regularizing functional of the form (43). The minimum of the functional $\tilde{F}$ is found at the zero of the gradient, i.e., from solving $\tilde{F}'(p)|_{p=p_{k+1}} = 0$ we get the next estimate p_{k+1}

$$\begin{aligned} p_{k+1} &= p_k + (J^T L_w^T L_w J + \alpha L^T L)^{-1}(J^T L_w^T L_w(y - G(p_k)) - \alpha L^T L(p_k - p_*)) \\ &\equiv p_k + \delta p^k. \end{aligned} \tag{46}$$

Often an additional step size parameter is used to control the iteration. The new estimate is obtained from $p_{k+1} = p_k + s_k \delta p^k$, where s_k is the step size parameter to be determined and δp^k is used as a search direction. This method is sometimes

called the *damped Gauss-Newton* method [104, 105]. The step size parameter can be determined, e.g., from a one-dimensional line search.

The *Levenberg-Marquardt* (LM) method is obtained likewise from a sequence of local linearizations and minimizations. For the Levenberg-Marquardt method, the search direction δp^k is solved by minimizing

$$\tilde{F}_{\mathrm{LM}}(\delta p) = ||L_w(y - G(p_k) - J\delta p)||^2 + \lambda||\delta p||^2, \tag{47}$$

and the next estimate is obtained as

$$p_{k+1} = p_k + \delta p^k = p_k + (J^T L_w^T L_w J + \lambda I)^{-1}(J^T L_w^T L_w(y - G(p_k)). \tag{48}$$

The Levenberg-Marquardt method originates from trust-region methods (see, e.g., [105]). The least squares problem (47) is related to a least squares problem of minimizing $||L_w(y-G(p_k)-J(\delta p))||^2$ with a quadratic constraint $||\delta p||^2 \leq \delta_c$, where the set of vectors δp satisfying $||\delta p||^2 \leq \delta_c$ is viewed as the region of trust for the linearizing approximation $G(p) \approx G(p_k) + J\delta p$ around the current estimate p_k. The choice of the parameter λ can be done based on the trust-region parameter δ_c [105]; however, in this work the LM algorithm was implemented by choosing λ based on visual inspection of the obtained estimate.

4.3 About statistical inversion methods

This section presents some basic concepts of statistical inversion theory and some results used in this thesis. The text is mainly based on [108].

4.3.1 General concepts

In statistical inversion theory, the parameters are divided into parameters that can be observed and parameters that are not directly observable. All the parameters are modelled as random variables that depend on each other through a model. The information on the parameter values is expressed by probability distributions. In the inverse problem, some of the unobservable parameters are of primary interest, whereas others are considered to be of secondary interest. The interdependence of the parameters is expressed through a joint probability distribution. The idea is then to make inference on the unknown parameters of interest based on all the knowledge of the measurements, the model between the parameters, and the prior information on the parameters. The solution of the inverse problem is the posterior probability distribution of the parameter of interest rather than a single estimate like in the traditional approach.

In the following, we give some basic ideas of the statistical approach to inverse problems. We denote the directly observable quantity, i.e., the measurement, by Y,

and the nonobservable quantity by X. Assuming a discretized model, Y and X are vector valued random variables, and we denote their realizations by y and x, respectively. The information on the nonobservable quantity X prior to the measurement is expressed by the prior probability density $\pi_{\mathrm{pr}}(x)$. The conditional probability density of the measurement Y given the value $X = x$ of the nonobservable quantity X is

$$\pi(y|x) = \frac{\pi(x,y)}{\pi_{\mathrm{pr}}(x)}, \quad \pi(x)_{\mathrm{pr}} > 0, \tag{49}$$

where $\pi(x,y)$ denotes the joint probability density of X and Y. The conditional probability density of the measurement is often called the *likelihood density*. The conditional probability density of X given the measurement data $Y = y$ is written as

$$\pi(x|y) = \frac{\pi(x,y)}{\pi(y)}, \quad \pi(y) > 0, \tag{50}$$

where $\pi(y) = \int \pi(x,y)dx$ is the *marginal probability density* of the measurement Y. Using Eq. (49) we may write the conditional probability density of X as

$$\pi(x|y) = \frac{\pi(y|x)\pi_{\mathrm{pr}}(x)}{\pi(y)}. \tag{51}$$

Equation (51) is a central theorem in statistical or *Bayesian* approach for inverse problems and is known as the *Bayes formula*. The conditional probability density of X is often referred to as the *posterior density* $\pi_{\mathrm{post}}(x)$ of X, and in statistical framework, it is the solution to the inverse problem. Given the measurement data y, the term $\pi(y)$ is a constant that is often left out; hence we write $\pi_{\mathrm{post}}(x) = \pi(x|y) \propto \pi(y|x)\pi_{\mathrm{pr}}(x)$.

In Bayesian approach, the solution to the inverse problem is a probability distribution rather than a single estimate. Obviously, a probability distribution contains more information on the solution than a single estimate; however, it is often useful to review or visualise single point estimates. There are several point estimates that may be drawn from the posterior distribution. One of the most commonly used is the *maximum a posterior* (MAP) estimate, that is defined by

$$x_{\mathrm{MAP}} = \arg\max_x \pi(x|y). \tag{52}$$

Computing the MAP estimate corresponds to solving an optimization problem. Another popular point estimate is the *conditional mean* (CM) estimate, that requires the solution of an integration problem

$$x_{\mathrm{CM}} = \int x\pi(x|y)dx. \tag{53}$$

Finally, we mention the *maximum likelihood* (ML) estimate, that corresponds to finding the value of X that is most likely to produce the data y

$$x_{\mathrm{ML}} = \arg\max_x \pi(y|x). \tag{54}$$

The ML estimate corresponds to solving the inverse problem without regularization, and in the case of ill-posed inverse problems it is quite unstable. In addition to point estimates, *interval estimates* can be retrieved from the posteriori distribution that help to assess the credibility of the estimates (c.f. [108]).

4.3.2 Additive Gaussian noise: Relation to the traditional approach

In order to form the posterior distribution, one must construct the likelihood function $\pi(y|x)$. The likelihood function is constructed using knowledge on the forward model and the characteristics of the noise and other measurement and modelling uncertainties. Assuming an observation model of the general form $Y = G(X, N)$, where Y is again a vector containing the measurement, X a vector of the unknown parameter values, and N the noise vector, the likelihood density is written as $\pi(y|x, n) = \delta(y - G(x, n))$, i.e., the model G completely defines the measurement Y.

A commonly used model for noise in applications is to assume that the noise is additive and that the noise N and the unknown parameters X are mutually independent. Then, we have a model

$$Y = G(X) + N. \tag{55}$$

Assume that the probability distribution of the noise $\pi_{\text{noise}}(n)$ is known. From (55) we have $N = Y - G(X)$, and further, if we fix $X = x$ we have $N = Y - G(x)$. Hence we deduce that $Y - G(x)$ follows the same distribution as the noise N, i.e., the probability density of Y conditioned on x is given by

$$\pi(y|x) = \pi_{\text{noise}}(y - G(x)). \tag{56}$$

Using the Bayes formula, we then have for the posterior density of X

$$\pi(x|y) \propto \pi_{\text{noise}}(y - G(x))\pi_{\text{pr}}(x). \tag{57}$$

Let us now consider the special case where the noise is Gaussian and of zero mean, i.e.,

$$\pi_{\text{noise}}(n) \propto \exp\left\{-\frac{1}{2}(n - n_0)^T \Gamma_{\text{noise}}^{-1}(n - n_0)\right\}, \tag{58}$$

where Γ_{noise} is the noise covariance matrix and $n_0 = 0$. In the sequel, we denote Gaussian distributions as written above by $N \sim \mathcal{N}(n_0, \Gamma_{\text{noise}})$. Then we have for the likelihood density

$$\pi(y|x) \propto \exp\left\{-\frac{1}{2}(y - G(x))^T \Gamma_{\text{noise}}^{-1}(y - G(x))\right\}. \tag{59}$$

The ML estimate x_{ML} is obtained by minimizing $\frac{1}{2}(y - G(x))^T \Gamma_{\text{noise}}^{-1}(y - G(x))$. Choosing $\frac{1}{2}\Gamma_{\text{noise}}^{-1} = L_w^T L_w$ we note that finding the ML estimate corresponds to

the weighted least squares estimation without regularization. Further, if the prior density of X is of the form $\pi_{\text{pr}}(x) \propto \exp(-\alpha f(x))$, we get for the posterior density

$$\pi(x|y) \propto \exp\left\{-\frac{1}{2}(y - G(x))^T \Gamma_{\text{noise}}^{-1}(y - G(x)) - \alpha f(x)\right\}. \tag{60}$$

The MAP estimate is obtained by minimizing $\frac{1}{2}(y-G(x))^T\Gamma_{\text{noise}}^{-1}(y-G(x))+\alpha f(x)$ which, choosing $\frac{1}{2}\Gamma_{\text{noise}}^{-1} = L_w^T L_w$, corresponds to the weighted least squares estimate with generalised Tikhonov regularization.

4.3.3 Gaussian prior densities

In this section, we present some results for the special case where the random variables in the model are Gaussian. Calculating, e.g., the Bayesian CM estimate is an integration problem that in general leads to computationally demanding integration using, e.g., Markov chain Monte Carlo (MCMC) methods. However, for Gaussian random variables we can derive closed form estimates for the means and covariances of the unknown parameters of interest. We restrict ourselves here to only presenting the most important results, and refer to the literature [108] for the proofs.

Consider a positive definite symmetric matrix

$$\begin{bmatrix} \Gamma_{11} & \Gamma_{12} \\ \Gamma_{21} & \Gamma_{22} \end{bmatrix} \in \mathbb{R}^{(n+k)\times(n+k)}, \tag{61}$$

where $\Gamma_{11} \in \mathbb{R}^{n\times n}$, $\Gamma_{22} \in \mathbb{R}^{k\times k}$, and $\Gamma_{21} = \Gamma_{12}^T$. First we define the Schur complements $\tilde{\Gamma}_{jj}$, $j = 1, 2$ by

$$\tilde{\Gamma}_{22} = \Gamma_{11} - \Gamma_{12}\Gamma_{22}^{-1}\Gamma_{21}, \quad \tilde{\Gamma}_{11} = \Gamma_{22} - \Gamma_{21}\Gamma_{11}^{-1}\Gamma_{12}. \tag{62}$$

Now, let $X \in \mathbb{R}^n$ and $Y \in \mathbb{R}^k$ be two Gaussian random variables with a joint probability density of the form

$$\pi(x, y) \propto \exp\left(-\frac{1}{2}\begin{bmatrix} x - x_0 \\ y - y_0 \end{bmatrix}^T \begin{bmatrix} \Gamma_{11} & \Gamma_{12} \\ \Gamma_{21} & \Gamma_{22} \end{bmatrix}^{-1} \begin{bmatrix} x - x_0 \\ y - y_0 \end{bmatrix}\right). \tag{63}$$

Then the conditional probability density of X conditioned on $Y = y$ is of the form

$$\pi(x|y) \propto \exp\left(-\frac{1}{2}(x - \bar{x})^T \tilde{\Gamma}_{22}^{-1}(x - \bar{x})\right), \tag{64}$$

where

$$\bar{x} = x_0 + \Gamma_{12}\Gamma_{22}^{-1}(y - y_0). \tag{65}$$

Further, the marginal density of X is

$$\pi(x) = \int_{\mathbb{R}^k} \pi(x,y)dy \propto \exp\left(-\frac{1}{2}(x-x_0)^T\Gamma_{11}^{-1}(x-x_0)\right). \tag{66}$$

The proofs of the above results are based on a matrix inversion lemma using Schur complements and may be found in [108].

Next, let us consider a linear model with additive noise,

$$Y = BX + N, \tag{67}$$

where $B \in \mathbb{R}^{m\times n}$ is known, and $X \in \mathbb{R}^n$ and $Y, N \in \mathbb{R}^m$ are random variables. Further, assume that X and N are mutually independent and Gaussian: $X \sim \mathcal{N}(x_0, \Gamma_{\text{pr}})$, $N \sim \mathcal{N}(n_0, \Gamma_{\text{noise}})$. Within these assumptions, the posterior density is then of the form $\pi(x|y) \propto \pi_{\text{pr}}(x)\pi_{\text{noise}}(y - Bx)$. To get a closed form estimate for X, we first form the joint probability density of X and Y, which by straightforward calculation assumes a form

$$\pi(x,y) \propto \exp\left(-\frac{1}{2}\begin{bmatrix} x-x_0 \\ y-y_0 \end{bmatrix}^T \begin{bmatrix} \Gamma_{\text{pr}} & \Gamma_{\text{pr}}B^T \\ B\Gamma_{\text{pr}} & B\Gamma_{\text{pr}}B^T + \Gamma_{\text{noise}} \end{bmatrix}^{-1} \begin{bmatrix} x-x_0 \\ y-y_0 \end{bmatrix}\right). \tag{68}$$

Hence, using the result in (64), we find that the posterior probability density of X conditioned on $Y = y$ is of the form

$$\pi(x|y) \propto \exp\left(-\frac{1}{2}(x-\bar{x})^T\Gamma_{\text{post}}^{-1}(x-\bar{x})\right), \tag{69}$$

where

$$\bar{x} = x_0 + \Gamma_{\text{pr}}B^T(B\Gamma_{\text{pr}}B^T + \Gamma_{\text{noise}})^{-1}(y - Bx_0 - n_0) \tag{70}$$

and

$$\Gamma_{\text{post}} = \Gamma_{\text{pr}} - \Gamma_{\text{pr}}B^T(B\Gamma_{\text{pr}}B^T + \Gamma_{\text{noise}})^{-1}B\Gamma_{\text{pr}}. \tag{71}$$

We note that in the Gaussian case the posterior distribution $\pi(x|y)$ is also Gaussian, and that the CM and MAP estimates coincide.

4.4 Estimation of absorption in anisotropic background

In this section, we summarize briefly the methods presented in the Publications of this thesis for the estimation of the optical absorption coefficient in the presence of anisotropies. Examples of the application of the estimation methods on simulated data are included at the end of this section and in the Publications. Let us also note that in these simulated examples, we have used anisotropies that are strong enough to give a significant effect on the data and hence also on the estimation. For example, the eigenvalues of the diffusion tensor are in most cases chosen so that

the larger eigenvalue is roughly three times the smaller one. There are no physical grounds for this choice but it is done in an *ad hoc* manner with the purpose to test the performance of the methods presented. Hence, the numerical results should be perceived with this aspect in mind.

4.4.1 Isotropic reconstruction

Let us first consider the estimation using a purely isotropic model for the anisotropic case. The isotropic least squares problem is to find μ_a and κ_0 that minimize a functional of a form

$$||y - G(\mu_\mathrm{a}, \kappa_0)||^2 + \alpha(f_{\mu_\mathrm{a}}(\mu_\mathrm{a}) + f_{\kappa_0}(\kappa_0)), \tag{72}$$

which in practice was solved using the Gauss-Newton or the Levenberg-Marquardt iteration. The performance of the isotropic method depends crucially on whether κ_0 is allowed to vary and develop significant boundary artefacts that compensate for the defective modelling. In such cases, the estimate of the absorption coefficient still contains some visible information on the main features, though the quality of the estimate is compromised by significant artefacts. However, if κ_0 is fixed, e.g., on the true value of the isotropic part of the body, and the estimation is conducted on μ_a only, the estimate of μ_a becomes totally useless. An example of applying isotropic reconstruction in an anisotropic case is presented in Fig. 3. Other examples of isotropic reconstructions may be found in Publications I, V, and VI.

4.4.2 Simultaneous reconstruction using partly fixed model

In the case structural prior information on anisotropies is available, one could in theory fix the direction of the anisotropy, and only reconstruct for the strength simultaneously with the absorption coefficient. The observation model is then written as

$$y = G(\mu_\mathrm{a}, \lambda_1, \lambda_2, \kappa_0) + n, \tag{73}$$

where n is additive noise and it is assumed that parts of the domain may be isotropic with an isotropic diffusion coefficient κ_0. The LS functional to be minimized then is of the form

$$||y - G(\mu_\mathrm{a}, \lambda_1, \lambda_2, \kappa_0)||^2 + \alpha(f_{\mu_\mathrm{a}}(\mu_\mathrm{a}) + f_{\lambda_1}(\lambda_1) + f_{\lambda_2}(\lambda_2) + f_{\kappa_0}(\kappa_0)). \tag{74}$$

As the recovery of spatially dependent $(\mu_\mathrm{a}, \lambda_1, \lambda_2, \kappa_0)$ may not be feasible, and the main interest is in the distribution of μ_a, in the numerical examples of this thesis (Publication IV) we have assumed that $(\lambda_1, \lambda_2, \kappa_0)$ are spatially constant. The estimation is done in two stages, where firstly we recover the constant scalar values of $(\mu_\mathrm{a}, \lambda_1, \lambda_2, \kappa_0)$, and secondly, move the iteration to a pixel basis for μ_a. The

results of the simulations in Publication IV show that as long as the geometry is modelled correctly, the estimation is fairly successful, but if the geometry is not accurately known, the quality of the estimates degrades relatively fast. As in reality the geometry would be known only up to certain accuracy, the practical applications of this approach are quite limited.

4.4.3 Calculation of the marginal density

Following the statistical approach presented in Sec. 4.3, our next approach consists of calculating the marginal posterior density of the absorption coefficient. In this section, we review briefly the calculation of the marginal posterior density in our application. Let us for now denote the anisotropy parameters $(\lambda_1, \lambda_2, \theta)$ by z. The observation model is thus

$$y = G(\mu_\mathrm{a}, z) + n, \tag{75}$$

where n again denotes additive measurement noise. The aim is to calculate the posterior density $\pi(\mu_\mathrm{a}, z|y)$ of $[\mu_\mathrm{a};\ z]$ conditioned on the measurement, and thereafter the marginal posterior density of μ_a by integrating the anisotropy parameters in z out. Assume now that μ_a, z and n are Gaussian and further that the noise n has zero mean: $\mu_\mathrm{a} \sim \mathcal{N}(\mu_{\mathrm{a},0}, \Gamma_{\mu_\mathrm{a}})$, $z \sim \mathcal{N}(z_0, \Gamma_z)$, $n \sim \mathcal{N}(0, \Gamma_\mathrm{noise})$. By linearizing the observation model at $[\mu_\mathrm{a}^*;\ z^*]$, we have $G(\mu_\mathrm{a}, z) \approx G(\mu_\mathrm{a}^*, z^*) + J_{\mu_\mathrm{a}}(\mu_\mathrm{a} - \mu_\mathrm{a}^*) + J_z(z - z^*) \equiv G(p^*) + J(p - p^*)$, where $J = [J_{\mu_\mathrm{a}}\ J_z]$ and $(p - p^*)^T = [(\mu_\mathrm{a} - \mu_\mathrm{a}^*)^T\ (z - z^*)^T]$. Thus, denoting $G(\mu_\mathrm{a}^*, z^*) = y^*$ we have a linearized observation model $y = y^* + J(p - p^*) + n$, which is of a similar form of Eq. (67) with $p \sim \mathcal{N}(p_0, \Gamma_p)$ and $p_0^T = [\mu_{\mathrm{a},0}^T\ z_0^T]$, $\Gamma_p = \mathrm{diag}(\Gamma_{\mu_\mathrm{a}}, \Gamma_z)$. Using the result in Eqs. (69)-(71) we see that $\pi(p|y) = \pi(\mu_\mathrm{a}, z|y)$ is Gaussian: $p \sim \mathcal{N}(\bar{p}, \Gamma_\mathrm{post})$, where

$$\bar{p} = \begin{bmatrix} \bar{\mu_\mathrm{a}} \\ \bar{z} \end{bmatrix} = \begin{bmatrix} \mu_{\mathrm{a},0} \\ z_0 \end{bmatrix} + \begin{bmatrix} \Gamma_{\mu_\mathrm{a}} J_{\mu_\mathrm{a}}^T \\ \Gamma_z J_z^T \end{bmatrix} L(y - y^* - J_{\mu_\mathrm{a}}(\mu_{\mathrm{a},0} - \mu_\mathrm{a}^*) - J_z(z_0 - z^*)) \tag{76}$$

and

$$\Gamma_\mathrm{post} = \begin{bmatrix} \Gamma_{\mu_\mathrm{a}} - \Gamma_{\mu_\mathrm{a}} J_{\mu_\mathrm{a}}^T L J_{\mu_\mathrm{a}} \Gamma_{\mu_\mathrm{a}} & -\Gamma_{\mu_\mathrm{a}} J_{\mu_\mathrm{a}}^T L J_z \Gamma_z \\ -\Gamma_z J_z^T L J_{\mu_\mathrm{a}} \Gamma_{\mu_\mathrm{a}} & \Gamma_z - \Gamma_z J_z^T L J_z \Gamma_z \end{bmatrix} \tag{77}$$

with

$$V = (J_{\mu_\mathrm{a}} \Gamma_{\mu_\mathrm{a}} J_{\mu_\mathrm{a}}^T + J_z \Gamma_z J_z^T + \Gamma_\mathrm{noise})^{-1}. \tag{78}$$

The probability density $\pi(\mu_\mathrm{a}, z|y)$ is a Gaussian density of the form of Eq. (63). The marginal density is now obtained in a straightforward manner by applying the result (66), and we have $\pi(\mu_\mathrm{a}|y) \propto \exp(-\frac{1}{2}(\mu_\mathrm{a} - \bar{\mu_\mathrm{a}})^T \Gamma_{\mathrm{post},\mu_\mathrm{a}}^{-1} (\mu_\mathrm{a} - \bar{\mu_\mathrm{a}}))$, where $\bar{\mu_\mathrm{a}}$ is as above and

$$\Gamma_{\mathrm{post},\mu_\mathrm{a}} = \Gamma_{\mu_\mathrm{a}} - \Gamma_{\mu_\mathrm{a}} J_{\mu_\mathrm{a}}^T V J_{\mu_\mathrm{a}} \Gamma_{\mu_\mathrm{a}}. \tag{79}$$

Note that the division of the parameters to μ_a and z is rather arbitrary. The parameter z can contain all the anisotropy parameters $(\lambda_1, \lambda_2, \theta)$ or only some of

them: the rest can be left out from the estimation problem by assuming that they are known and fixing their values. Also, in theory, the marginalization can be done with respect to any of the parameters giving the marginal posterior density of the rest. However, due to non-uniqueness issues of anisotropic inverse problems, an attempt to estimate the anisotropy in such a manner without essential prior knowledge is not guaranteed to be successful. In Publication I, simulated results using marginalization are calculated using simply $z = \lambda_2$ and assuming λ_1 and θ to be known.

4.4.4 Modelling error approach

Consider again an observation model of the form

$$y = G(\mu_\mathrm{a}, z) + n, \tag{80}$$

where n denotes the measurement noise, and the parameter z includes the unknown parameters of secondary interest. In this section, we present a method where unknown parameters of secondary interest are not included in the estimation explicitly, but fixed to a certain value z^*. Depending on the prior knowledge available on the quantities in z, the approximation $z = z^*$ may be more or less truthful; however, in general the uncertainty in value z^* can be considerable. The discrepancy between the true value and the value z^* induces an error into our model. In this approach, we aim to treat this modelling error as noise. Hence, we write the observation model as

$$y = G(\mu_\mathrm{a}, z^*) + (G(\mu_\mathrm{a}, z) - G(\mu_\mathrm{a}, z^*)) + n = G(\mu_\mathrm{a}, z^*) + \epsilon(\mu_\mathrm{a}, z) + n, \tag{81}$$

where the term $\epsilon(\mu_\mathrm{a}, z)$ represents modelling error due to the approximation $z = z^*$. From the point of the view of the statistical approach, if we had specified the prior knowledge on μ_a and z, we could in principle estimate the probability distribution of the modelling error term. However, at this point, we make again a strong simplification by resorting to linearization and Gaussian approximation. We make a local linearization at the current estimate $\mu_{\mathrm{a},k}$ of μ_a:

$$\epsilon(\mu_\mathrm{a}, z) \approx \epsilon(\mu_{\mathrm{a},k}, z) \approx J_z \delta z, \quad \delta z = z - z^*, \tag{82}$$

where J_z denotes the Jacobian matrix of the nonlinear mapping G with respect z at (μ_a, z)=$(\mu_{\mathrm{a},k}, z^*)$. The total error e is then

$$e = \epsilon + n \approx J_z \delta z + n. \tag{83}$$

Assuming that the noise and the parameters are mutually independent and Gaussian, $z \sim \mathcal{N}(z^*, \Gamma_z)$, $n \sim \mathcal{N}(0, \Gamma_\mathrm{noise})$, the covariance of the total error e becomes

$$\Gamma_e = E\{ee^T\} \approx J_z \Gamma_z J_z^T + \Gamma_\mathrm{noise}. \tag{84}$$

Hence the original model (80) is reduced to

$$y = G(\mu_{\mathrm{a}}, z^*) + e = G(\mu_{\mathrm{a}}) + e \tag{85}$$

with additive noise e with covariance Γ_e. To solve the related inverse problem, we can now apply any iterative estimation method such as least squares estimation of the form of, e.g., Eqs. (42) or (47) with $\Gamma_e^{-1} = L_w^T L_w$. A numerical example of the modelling error approach combined with LM estimation is presented in Fig. 3, and other examples are found in Publications V and VI. We note that the modelling error approach is essentially very similar to the calculation of marginal density. One advantage of this representation is that it provides an easy way to apply iterative estimation schemes on the absorption coefficient.

4.5 Geometrical mismodelling

Publication VI presents an application of the modelling error approach reviewed in the previous section to geometric mismodelling. Commonly in optical tomography the boundary shape and the optode locations of the domain being imaged are assumed to be known, and a fixed model is used for the reconstruction. However, generally the fixed model used is only an approximation to the reality, and the discrepancies between the model and reality may produce artefacts and compromise the quality of the reconstruction. How severe this degradation is likely to be depends on the type of application. In difference imaging, where two data sets with a fixed geometry are measured and the difference of these data are used for image reconstruction, the effects of geometric discrepancies may not be of major significance. On the contrary, in absolute imaging the reconstruction is done using a single set of data, and even slight disturbances may deteriorate the estimate significantly. Some recently emerged algorithms such as optode positional calibration [109] or calibration for, e.g., the optode gains [110, 111] (though originally not intended specifically for geometric mismodelling) may help to take this problem into account. Publication VI presents another option by recasting geometric mismodelling into generation of anisotropies in an otherwise isotropic body.

The key idea of Publication VI is to represent geometric mismodelling using a diffeomorphic mapping from the model to the reality. Let us denote the real physical domain by Ω, and the model domain that we use for reconstruction by Ω'. Also, we assume that there is a one-to-one mapping $\Upsilon : \Omega' \to \Omega$ such that Υ as well as its inverse $\Upsilon^{-1} : \Omega \to \Omega'$ are differentiable, and furthermore, we assume that Υ maps the boundary $\partial\Omega'$ to $\partial\Omega$. Now, one can deduce that if $\Phi(\mathbf{r})$ satisfies the diffusion equation (29) in Ω, in Ω' there exists a corresponding function Φ' for which $\Phi(\mathbf{r}) = \Phi'(\mathbf{r}')$. Furthermore, $\Phi'(\mathbf{r}')$ also satisfies *a diffusion equation*, in which the original quantities κ, μ_{a} and q are deformed in such a manner that an originally isotropic κ may become anisotropic. The details of the proof and the deformations of the parameters can be found in Publication VI.

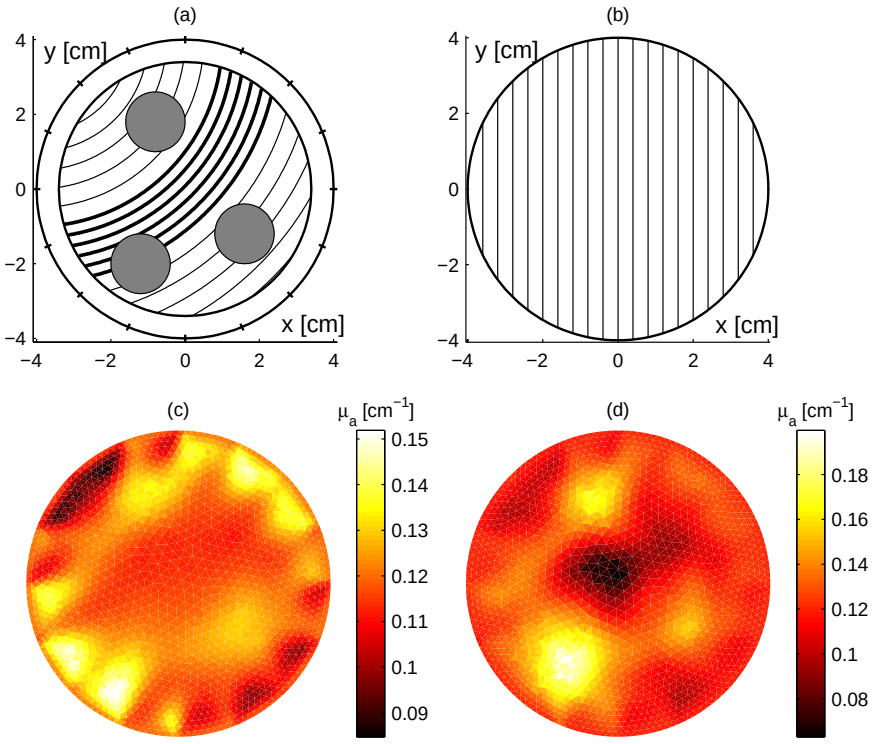

Figure 3: *Numerical example of the isotropic reconstruction and the modelling error approach in an anisotropic case. (a) The model used for data generation. The boundary is isotropic with* κ_0*=0.0495 cm*$^{-1}$ *and the central part anisotropic with the direction of anisotropy parallel to the lines and* (λ_1, λ_2)*=(0.0495 cm*$^{-1}$*, 0.0167 cm*$^{-1}$*), except for the stronger stripe in the middle where* (λ_1, λ_2)*=(0.0980 cm*$^{-1}$*, 0.0167 cm*$^{-1}$*). The background absorption* $\mu_{a,bg}$*=0.10 cm*$^{-1}$*, and the three gray spheres (radii 0.8 cm) represent three perturbations in* μ_a *with* μ_a*=0.20 cm*$^{-1}$*. Simulated data was collected using 16 source/measurement locations at equal distances on the boundary. The source is placed at each location at turn, and the rest of the locations are used for measurement, resulting into 240 data values for both of the measurement types* $\ln A$ *and* φ*. (b) The anisotropy model used in the modelling error approach. The direction of anisotropy is parallel to the* $y-$*axis and* (λ_1, λ_2)*= (0.0332 cm*$^{-1}$*, 0.0249 cm*$^{-1}$*). (c) The estimate of* μ_a *using an isotropic LM iteration for* μ_a *and* κ_0 *simultaneously. The starting point of the iteration was* (μ_a, κ_0)*=(0.05 cm*$^{-1}$*, 0.0495 cm*$^{-1}$*). First the background values were estimated, after which the iteration was continued in the FE pixel basis. (d) Reconstruction of* μ_a *using the modelling error approach with* $z = [\lambda_1; \lambda_2; \theta]$ *combined with LM iteration. In this example,* z^* *is as depicted in Fig. 3 (b),* σ_z*=*$[\sigma_{\lambda_1}; \sigma_{\lambda_2}; \sigma_\theta]$ *=[0.050 cm*$^{-1}$*; 0.050 cm*$^{-1}$*, 1.35 rad] and all parameter are discretized using the FE pixel basis. In LM iteration the starting point was* μ_a*=0.05 cm*$^{-1}$*, first the background value of* μ_a *was estimated, and secondly the iteration was moved into pixel basis.*

The approach taken in the estimation when the boundary shape and optode positions are not accurately known is to allow the domain to be anisotropic and reconstruct for the absorption coefficient only. Then we can pose a relatively loose model for the anisotropy and apply the modelling error approach to handle the possible anisotropies. Publication VI shows a numerical example of the generation of anisotropies in an isotropic body due to geometric mismodelling and the estimation of the absorption coefficient with geometric mismodelling using the modelling error approach.

5 Discussion

In this thesis, modelling and reconstruction methods for optical tomography were developed with a special emphasis on a situation where the medium is anisotropic. The anisotropic diffusion equation used for solving the forward problem of OT was derived, and the numerical solution using the FE method implemented. The FE solution to the anisotropic DE was compared to a MC simulation and to a BE solution to the DE.

The main focus in this thesis is, however, on the inverse problem of OT in the presence of anisotropies. There, the first point to consider is how to define the inverse problem in a feasible way. The excess of parameters in the anisotropic case poses questions such as which parameters to reconstruct and how to deal with the rest of the parameters of which, in a realistic application, there is a limited amount of information. The principal idea throughout this work is that the main interest in many applications is on the absorption coefficient. Hence, primarily the recovery of the absorption coefficient was strived for at the expense of the other parameters. In this thesis, a few different approaches were presented. In addition to the conventional isotropic reconstruction, another straightforward way is to fix some of the anisotropy parameters such as the structure of the body. The justification for this choice is that one is more likely to have prior information on the structure and the direction of anisotropy than the strength of the diffusion. However, numerical evidence shows that in this approach the accurate knowledge of the structure is critical for the success of the estimation. In light of the plausible prior knowledge that one might have, the statistical treatment of anisotropies is probably the most realistic one. The statistical approach enables modelling of anisotropies using probability distributions, which is well in accordance with having information on the main features of the structure and plausible intervals of the strength. The numerical examples in this thesis show that statistical inversion methods can help to improve the quality of the estimates even with very limited prior knowledge on the background anisotropy.

The numerical work in this thesis was conducted in 2D. However, modelling and reconstruction from real data generally require a 3D model to be successful. The work in this thesis should be taken as a "proof-of-concept". Studying, implementing and testing novel methods is much easier and faster in 2D than in 3D. Moving into 3D increases the dimension of the numerical problem substantially, which requires special attention to the implementation and increases the computational load significantly. However, in order to test the methods on real data, a 3D implementation is a necessary as well as an advisable part of future work.

In this work, the implementation of the statistical methods was done using rather restrictive simplifications on the parameter distributions. Gaussian approximations enabled the derivation of the sought estimates in a closed form. However, the prospects in statistical inversion methods are much wider. In the statistical ap-

proach, it is possible to pose a realistic probabilistic model for the unknown parameters. Generally, calculation of the point estimates and assessing their confidence then becomes a numerical integration problem that requires specific methods such as stochastic simulation using MCMC techniques.

The role of anisotropy in OT is an interesting question yet not very well understood. How strongly the anisotropic tissue structures, e.g., in the brain show in the data as well as in the results of the estimation is a subject that would need further research. Preliminary MC simulations in the infant head indicate that the effect on the data might be notable. However, the true measured data will have many sources of interference, the effects of which might be relatively large compared to the effects of anisotropies. The role of anisotropies is not, however, limited to physical anisotropic tissue structures. As indicated in Publication VI, anisotropies could be used to model other phenomena as well. The anisotropic diffusion model provides a computationally feasible tool to model anisotropic phenomena. Together with the statistical approach they could help to overcome problems related to, e.g., uncertainties in the geometry by simply *allowing* for the presence of anisotropies.

Summary of publications

I Estimation of optical absorption in anisotropic background (Inverse Problems 18:559-573, 2002).

This publication introduces optical anisotropies in the context of medical optical tomography. In the first part of the publication, the diffusion equation is derived in its anisotropic form together with the boundary conditions. A numerical implementation in 2D using the FE method is then presented. In the latter part of the paper, the inverse problem of the estimation of the optical absorption coefficient in the presence of anisotropies is considered. More specifically, a case where the direction and the strength of the anisotropy are constant and the strength is assumed unknown is studied. Two approaches for the estimation are presented. The first one attempts to recover the MAP estimate assuming a fixed isotropic or anisotropic background, and it is found that the estimation is successful only when the truthful information of the background anisotropy is assumed. In the second approach, following the Bayesian thinking, the marginal posterior density for the absorption in condition of the measurements is calculated. The unknown absorption and anisotropy parameters are assigned Gaussian prior distributions, and linearizing the observation model, the formula for the MAP estimate is derived without having to use numerical integration. In this case, the estimates of the absorption coefficient are considerably better even if the prior information on the strength of the anisotropy is very weak.

II Anisotropic effects in highly scattering media (Physical Review E 68, 031908, 2003).

This paper considers anisotropic scattering and light propagation models both theoretically and using numerical simulations. Firstly, a possible anisotropic scattering phase function is constructed. The derivation of the diffusion approximation using both isotropic and anisotropic phase functions is briefly reviewed. The rest of the paper deals with numerical experiments using a Monte Carlo simulation based on the radiative transfer model, and finite element and boundary element methods implementing the numerical solution of the diffusion equation. The models are constructed using a simple choice of anisotropy, and the derived anisotropy model then allows for the comparison of the results from the different numerical approaches. The data from each simulation were found to agree relatively well.

III Diffuse optical imaging (James Lin (ed.), Advances in Electromagnetic Fields in Living Systems, Vol. 4, 77-130, Springer Science 2005, in press).

This publication is a review-type book chapter addressing the physiological background, modelling and reconstruction methods, instrumentation, experimental methods and applications of medical optical imaging.

IV Simultaneous estimation of optical anisotropy and absorption in medical optical tomography (Proceedings of IVth International Workshop - Computational Problems of Electrical Engineering, Zakopane, Poland. 191-194, 2002).

This publication presents the reconstruction of the optical absorption coefficient simultaneously with the anisotropic strength parameters when the background anisotropic structure is either well known or differs only slightly from the reality. The constant isotropic diffusion coefficient of the isotropic areas is included in the reconstruction. The quality of the estimates decreases relatively fast with the accuracy of the underlying model for the structures. Generally, the structural information on anisotropies, if available, may not be very accurate, implying that further work should be done to overcome this problem.

V A modelling error approach for the estimation of optical absorption in the presence of anisotropies (Physics in Medicine and Biology 49:4785-4798, 2004).

This paper is concerned with a situation in optical tomography, where information on the background anisotropy is poor. The goal is to estimate the distribution of optical absorption. The rest of the unknown parameters, in this case the anisotropic diffusion parameters, are treated as modelling errors and included into the estimation scheme. The prior information used for anisotropy parameters is a relatively wide distribution of the plausible values the parameters may take. The paper presents numerical examples comparing reconstructions in an unknown anisotropic background using either an isotropic inversion scheme or the modelling error approach. Using the modelling error approach, the inhomogeneities in the absorption coefficient are more clearly visible than with a conventional isotropic model.

VI Compensation of geometric mismodelling by anisotropies in optical tomography (Optics Express 13:296-308, 2005).

This paper presents the application of the modelling error approach presented in Publication V on geometric mismodelling. In optical tomography, the boundary of the body and the optode positions can only be known up to a certain accuracy. The reconstruction is often done using a fixed model for the geometry, and the discrepancies between the model and reality lead to artefacts. We see that geometric mismodelling in an isotropic case may correspond to an anisotropic model. By allowing the domain to be anisotropic and applying the modelling error approach during the estimation, the quality of the obtained estimate may be improved.

Author's contribution

All publications are result of shared work with the co-authors. Throughout the publications (excluding Publication III), the contribution of the author of this thesis has been mainly on the implementation and testing of the numerical calculations, especially using the finite element method. In more detail, in Publication I the author was responsible for the designing and implementation of the numerical calculations and writing parts related to that. In Publication II, the author conducted the FEM calculations, implemented the anisotropic Monte Carlo code based on an isotropic version in collaboration with the second author and conducted the Monte Carlo simulations. The paper was composed by the author using notes (the scattering phase functions and representation of the anisotropic diffusion equation in Sec. II, and Secs. III C and D) from co-authors. In Publication III, the author was responsible for writing Sec. 3 on theory and modelling in optical tomography, and gave some contribution to the introduction and discussion. In Publication IV, the author was responsible for designing and implementing the numerical calculations and, for the most part, writing the publication. In Publication V, the author implemented and tested the numerical calculations and wrote most of the manuscript, apart from some paragraphs on the LM-algorithm and modelling errors, the conclusion, and some editing. In Publication VI, the author conducted the numerical work. The manuscript was written by the author apart from Sec. 2.1, part of the conclusions, the appendix, and some editing.

References

[1] V. Ntziachristos, X. Ma, and B. Chance. Time-correlated single photon counting imager for simultaneous magnetic resonance and near-infrared mammography. *Rev. Sci. Instrum.* **69**, 4221-4233 (1998).

[2] H. Eda, I. Oda, Y. Ito, Y. Wada, Y. Oikawa, Y. Tsunazawa, M. Takada, Y. Tsuchiya, Y. Yamashita, M. Oda, A. Sassaroli, Y. Yamada, and M. Tamura. Multichannel time-resolved optical tomographic imaging system. *Rev. Sci. Instrum.* **70**, 3595-3601 (1999).

[3] F. E. W. Schmidt, M. E. Fry, E. M. C. Hillman, J. C. Hebden, and D. T. Delpy. A 32-channel time-resolved instrument for medical optical tomography. *Rev. Sci. Instrum.* **71**, 256-265 (2000).

[4] I. Nissilä, K. Kotilahti, K. Fallström, and T. Katila. Instrumentation for the accurate measurement of phase and amplitude in optical tomography. *Rev. Sci. Instrum.* **73**, 3306-3312 (2002).

[5] T. O. McBride, B. W. Pogue, S. Jiang, U. L. Österberg, and K. D. Paulsen. A parallel-detection frequency-domain near-infrared tomography system for hemoglobin imaging of the breast in vivo. *Rev. Sci. Instrum.* **72**, 1817-1824 (2001).

[6] S. R. Arridge, M. Cope, and D. T. Delpy. The theoretical basis for the determination of optical pathlengths in tissue: temporal and frequency analysis. *Phys. Med. Biol.* **37**, 1531-1560 (1992).

[7] J. C. Schotland and V. A. Markel. Inverse scattering with diffusing waves. *J. Opt. Soc. Am. A* **18**, 2767-2777 (2001).

[8] V. A. Markel and J. C. Schotland. Inverse problem in optical diffusion tomography. I. Fourier-Laplace inversion formulas. *J. Opt. Soc. Am. A* **18**, 1336-1347 (2001).

[9] S. C. Walker, S. Fantini and E. Gratton. Image reconstruction by backprojection from frequency-domain optical measurements in highly scattering media. *Appl. Opt.* **36**, 170-179 (1997).

[10] S. B. Colak, D. G. Papaioannou, G. W 't Hooft, M. B. van der Mark, H. Schomberg, J. C. J. Paasschens, J. B. M. Melissen and N. A. A. J. van Asten. Tomographic image reconstruction from optical projections in light-diffusing media. *Appl. Opt.* **36**, 180-213 (1997).

[11] C. L. Matson and H. Liu. Backpropagation in turbid media. *J. Opt. Soc. Am. A* **16**, 1254-1265 (1999).

[12] M. A. O'Leary, D. A. Boas, B. Chance, and A. G. Yodh. Experimental images of heterogeneous turbid media by frequency-domain diffusing-photon tomography. *Opt. Lett.* **20**, 426-428 (1995).

[13] V. Kolehmainen, S. R. Arridge, M. Vauhkonen, and J. P. Kaipio. Simultaneous reconstruction of internal tissue region boundaries and coefficients in optical diffusion tomography. *Phys. Med. Biol.* **45**, 3267-3283 (2000).

[14] V. Kolehmainen. *Novel approaches to image reconstruction in diffusion tomography.* PhD Thesis, Univ. of Kuopio (2001).

[15] N. Hyvönen. Characterizing inclusions in optical tomography. *Inv. Probl.* **20**, 737-751 (2004).

[16] J. C. Hebden. Advances in optical imaging of the newborn infant brain. *Phychophysiology* **40**, 501-510 (2003).

[17] H. Obrig and A. Villringer. Beyond the visible – Imaging of the human brain with light. *J. Cereb. Blood Flow Metab.* **23**, 1-18 (2003).

[18] J. C. Hebden, A. Gibson, R. M. Yusof, N. Everdell, E. M. C. Hillman, D. T. Delpy, S. R. Arridge, T. Austin, J. H. Meek, and J. S. Wyatt. Three-dimensional optical tomography of the premature infant brain. *Phys. Med. Biol.* **47**, 4155-4166 (2002).

[19] J. C. Hebden, A. Gibson, T. Austin, R. M. Yusof, N. Everdell, D. T. Delpy, S. R. Arridge, J. H. Meek, and J. S. Wyatt. Imaging changes in blood volume and oxygenation in the newborn infant brain using three-dimensional optical tomography. *Phys. Med. Biol.* **49**, 1117-1130 (2004).

[20] M. A. Franceschini, V. Toronov, M. E. Filiaci, E. Gratton, and S. Fantini. On-line optical imaging of the human brain with 160 ms temporal resolution. *Opt. Expr.* **6**, 49-57 (2000).

[21] R. P. Kennan, S. G. Horovitz, A. Maki, Y. Yamashita, H. Koizumi, and J. C. Gore. Simultaneous recording of event-related auditory oddball response using transcranial near infrared optical topography and surface EEG. *NeuroImage* **16**, 587-592 (2002).

[22] H. Sato, T. Takeuchi, and K. L. Sakai. Temporal cortex activation during speech recognition: an optical topography study. *Cognition* **73**, B55-66 (1999).

[23] B. Chance, E. Anday, S. Nioka, S. Zhou, L. Hong, K. Worden, C. Li, T. Murray, Y. Ovetsky, D. Pidikiti, and R. Thomas. A novel method for fast imaging of brain function, non-invasively, with light. *Opt. Expr.* **2**, 411-423 (1998).

[24] Y. Chen, S. Zhou, C. Xie, S. Nioka, M. Delivoria-Papadopoulos, E. Anday, and B. Chance. Preliminary evaluation of dual wavelength phased array imaging on neonatal brain function. *J. Biomed. Opt.* **5**, 194-200 (2000).

[25] S. R. Hintz, D. A. Benaron, A. M. Siegel, A. Zourabian, D. K. Stevenson, and D. A. Boas. Bedside functional imaging of the premature infant brain during passive motor activation. *J. Perinat. Med.* **29**, 335-343 (2001).

[26] G. Taga, K. Asakawa, A. Maki, Y. Konishi, and H. Koizumi. Brain imaging in awake infants by near-infrared optical topography. *Proc. Natl. Acad. Sci. U S A* **100**, 10722-10727 (2003).

[27] B. W. Pogue, S. P. Poplack, T. O. McBride, W. A. Welss, K. S. Osterman, U. L. Ostenberg, and K. D. Paulsen. Quantitative hemoglobin tomography with diffuse near-infrared spectroscopy: Pilot results in the breast. *Radiology* **218**, 261-266 (2001).

[28] H. Dehghani, B. W. Pogue, S. P. Poplack, and K. D. Paulsen. Multiwavelength three-dimensional near-infrared tomography of the breast: initial simulation, phantom, and clinical results. *Appl. Opt.* **42**, 135-145 (2003).

[29] N. G. Chen, M. Huang, H. Xia, D. Piao, E. Cronin, and Q. Zhu. Portable near-infrared diffusive light imager for breat cancer detection. *J. Biomed. Opt.* **9**, 504-510 (2004).

[30] E. M. C. Hillman, J. C. Hebden, M. Schweiger, H. Dehghani, F. E. W. Schmidt, D. T. Delpy, and S. R. Arridge. Time resolved optical tomography of the human forearm. *Phys. Med. Biol.* **46**, 1117-1130 (2001).

[31] M. Niwayama, K. Yamamoto, D. Kohota, K. Hirai, N. Kudo, T. Hamaoka, R. Kime, and T. Katsumura. A 200-channel imaging system of muscle oxygenation using CW near-infrared spectroscopy. *IEICE Trans. Inf. & Syst.* **85-D**, 115-123 (2002).

[32] J. Riley, H. Dehghani, M. Schweiger, S. R. Arridge, J. Ripoll, and M. Nieto-Vesperinas. 3D optical tomography in the presence of void regions. *Opt. Expr.* **7**, 462-467 (2000).

[33] S. R. Arridge, H. Dehghani, M. Schweiger, and E. Okada. The finite element model for the propagation of light in scattering media: A direct method for domains with nonscattering regions. *Med. Phys.* **27**, 252-264 (2000).

[34] H. Dehghani, S. R. Arridge, M. Schweiger, and D. T. Delpy. Optical tomography in the presence of void regions. *J. Opt. Soc. Am. A* **17**, 1659-1670 (2000).

[35] N. Hyvönen. Analysis of optical tomography with non-scattering regions. *Proceedings of the Edinburgh Mathematical Society* **45**, 257-276 (2002).

[36] T. Tarvainen, M. Vauhkonen, V. Kolehmainen, and J. P. Kaipio. A hybrid radiative transfer - diffusion model for optical tomography. *Appl. Opt.* **44**, 876-886 (2005).

[37] L. Wang and S. L. Jacques. Hybrid model of Monte Carlo simulation and diffusion theory for light reflectance by turbid media. *J. Opt. Soc. Am. A* **10**, 1746-1752 (1993).

[38] H. Jiang. Optical image reconstruction based on the third-order diffusion equations. *Opt. Expr.* **4**, 241-246 (1999).

[39] D. Le Bihan, J-F. Mangin, C. Poupon, C. A. Clark, S. Pappata, N. Molko, and H. Chabriat. Diffusion tensor imaging: Concepts and applications. *Journal of Magnetic Resonance Imaging* **13**, 534-546 (2001).

[40] D. S. Tuch, V. J. Wedeen, A. M. Dale, J. S. George, and J. W. Belliveau. Conductivity tensor mapping of the human brain using diffusion tensor MRI. *Proc. Nat. Acad. Sci.* **98**, 11697-11701 (2001).

[41] R. Aaron, M. Huang, and C. A. Shiffman. Anisotropy of human muscle via non-invasive impedance measurements. *Phys. Med. Biol.* **42**, 1245-1262 (1997).

[42] F. X. Hart, N. J. Berner, and R. L. McMillen. Modelling the anisotropic electrical properties of skeletal muscle. *Phys. Med. Biol.* **44**, 413-421 (1999).

[43] G. Marquez, L. V. Wang, S. Lin, J. A. Schwartz, and S. L. Thomsen. Anisotropy in the absorption and scattering of chicken breast tissue. *Appl. Opt.* **37**, 798-804 (1998).

[44] A. Kienle, F. K. Forster, R. Diebolder, and R. Hibst. Light propagation in dentin: influence of microstructure on anisotropy. *Phys. Med. Biol.* **48**, N7-N14 (2003).

[45] S. Nickell, M. Hermann, M. Essenpreis, T. J. Farrell, U. Krämer, and M. S. Patterson. Anisotropy of light propagation in human skin. *Phys. Med. Biol.* **45**, 2873-2886 (2000).

[46] C. R. Tench, P. S. Morgan, M. Wilson, and L. D. Blumhardt. White matter mapping using diffusion tensor MRI. *Magnetic Resonance in Medicine* **47**, 967-972 (2002).

[47] P. J. Basser, S. Pajevic, C. Pierpaoli, J. Duda, and A. Aldroubi. In vivo fiber tractography using DT-MRI data. *Magnetic Resonance in Medicine* **44**, 625-632 (2000).

[48] J. Heiskala, I. Nissilä, T. Neuvonen, S. Järvenpää, and E. Somersalo. Modeling anisotropic light propagation in a realistic model of the human head. *Appl. Opt.* **44**, 2049-2057 (2005).

[49] J. Heiskala, Biomag Laboratory, Helsinki Univ. Central Hospital. Private communication.

[50] L. Dagdug, G. H. Weiss, and A. H. Gandjbakhche. Effects of anisotropic optical properties on photon migration in structured tissues. *Phys. Med. Biol.* **48**, 1361-1370 (2003).

[51] O. K. Dudko, G. H. Weiss, V. Chernomordik, and A. H. Gandjbakhche. Photon migration in turbid media with anisotropic optical properties. *Phys. Med. Biol.* **49**, 3979-3989 (2004).

[52] J. C. Hebden, J. J. G. Guerrero, V. Chernomordik, and A. H. Gandjbakhche. Experimental evaluation of an anisotropic scattering model of a slab geometry. *Opt. Lett.* **29**, 2518-2520 (2004).

[53] J. Heino, S. Arridge, and E. Somersalo. Anisotropic effect in light scattering and some implications in optical tomography. *OSA Biomedical Topical Meetings, OSA Technical Digest*, 18-20 (Optical Society of America, Washington DC, 2002).

[54] S. Arridge. Diffusion tomography in dense media. *Scattering and Inverse Scattering in Pure and Applied Science* **1**, 920-936 (Ed. R. Pike and P. Sabatier, Academic Press, 2002).

[55] S. Chandrasekhar. *Radiative Transfer* (Oxford University Press, London, 1950).

[56] M. C. Case and P. F. Zweifel *Linear Transport Theory* (New York: Addison-Wesley, 1967).

[57] S. R. Arridge. Optical tomography in medical imaging. *Inv. Probl.* **15**, R41-R93 (1999).

[58] D. A. Boas. *Diffuse photon probes of structural and dynamical properties of turbid media: Theory and biomedical applications.* PhD Thesis, Univ. of Pennsylvania (1996).

[59] L. G. Henyey and J. L. Greenstein. Diffuse radiation in the galaxy. *Astro-Phys. J.* **93**, 70-83 (1941).

[60] A. Ishimaru. *Wave Propagation and Scattering in Random Media, VOLUME 1, Single Scattering and Transport Theory.* (Academic Press, 1978).

[61] R. C. Haskell, L. O. Svaasand, T-T. Tsay, T-C. Feng, M. S. McAdams, and B. J. Tromberg. Boundary conditions for the diffusion equation in radiative transfer. *J. Opt. Soc. Am. A* **11**, 2727-2741 (1994).

[62] J. B. Fishkin and E. Gratton. Propagation of photon-density waves in strongly scattering media containing an absorbing semi-infinite plane bounded by a straight edge. *J. Opt. Soc. Am. A* **10**, 127-140 (1993).

[63] A. H. Hielscher, R. E. Alcouffe and R. L. Barbour. Comparison of finite-different transport and diffusion calculations for photon migration in homogeneous and heterogeneous tissues. *Phys. Med. Biol.* **43**, 1285-1302 (1998).

[64] A. D. Kim and A. Ishimaru. Optical diffusion of continuous-wave, pulsed, and density waves in scattering media and comparisons with radiative transfer. *Appl. Opt.* **37**, 5313-5319 (1998).

[65] E. Okada, M. Schweiger, S. R. Arridge, M. Firbank, and D. T. Delpy. Experimental validation of Monte Carlo and finite-element methods for the estimation of the optical path length in inhomogeneous tissue. *Appl. Opt.* **35**, 3362-3371 (1996).

[66] E. Okada, M. Firbank, M. Schweiger, S. R. Arridge, M. Cope, and D. T. Delpy. Theoretical and experimental investigation of near-infrared light propagation in a model of the adult head. *Appl. Opt.* **36**, 21-31 (1997).

[67] S. R. Arridge, M. Schweiger, M. Hiraoka, and D. T. Delpy. A finite element approach for modeling photon transport in tissue. *Med. Phys.* **20**, 299-309 (1993).

[68] M. Schweiger, S. R. Arridge, M. Hiraoka, and D. T. Delpy. The finite element method for the propagation of light in scattering media: Boundary and source conditions. *Med. Phys.* **22**, 1779-1792 (1995).

[69] T. Durduran, D. A. Boas, B. Chance, and A. G. Yodh. Validity of the diffusion equation for small heterogeneities. *OSA TOPS on Advances in Optical Imaging and Photon Migration* **2**, 60-65 (Ed. R. R. Alfano and J. G. Fujimoto, 1996).

[70] M. Schweiger and S. R. Arridge. Optimal data types in optical tomography. *Information Processing in Medical Imaging (IPMI'97 Proceedings) (Lecture notes in Computer Science 1230)*, 71-84 (1997).

[71] F. Gao, H. Zhao, and Y. Yamada. Improvement of image quality in diffuse optical tomography by use of full time-resolved data. *Appl. Opt.* **41**, 778-791 (2002).

[72] E. M. C. Hillman, J. C. Hebden, F. E. W. Schmidt, S. R. Arridge, M. Schweiger, H. Dehghani, and D. T. Delpy. Calibration techniques and datatype extraction for time-resolved optical tomography. *Rev. Sci. Instrum.* **71**, 3415-3427 (2000).

[73] B. W. Pogue, M. S. Patterson, H. Jiang, and K. D. Paulsen. Initial assessment of a simple system for frequency domain diffuse optical tomography. *Phys. Med. Biol.* **40**, 1709-1729 (1995).

[74] Y. Yao, Y. Wang, Y. Pei, W. Zhu, and R. Barbour. Frequency-domain optical imaging of absorption and scattering distributions by a Born iterative method. *J. Opt. Soc. Am. A* **14**, 325-342 (1997).

[75] M. J. Eppstein, D. E. Dougherty, T. L. Troy, and E. M. Sevick-Muraca. Biomedical optical tomography using dynamic parametrization and Bayesian conditioning on photon migration measurements. *Appl. Opt.* **38**, 2138-2150 (1999).

[76] A. H. Hielscher, A. D. Klose, and K. M. Hanson. Gradient-based iterative image reconstruction scheme for time-resolved optical tomography. *IEEE Transactions on Medical Imaging* **18**, 262-271 (1999).

[77] V. Ntziachistos, A. H. Hielscher, A. G. Yodh, and B. Chance. Diffuse optical tomography of highly heterogeneous media. *IEEE Transactions on Medical Imaging* **20**, 470-478 (2001).

[78] M. Schweiger and S. R. Arridge. The finite-element method for the propagation of light in scattering media: Frequency domain case. *Med. Phys.* **24**, 895-902 (1997).

[79] S. R. Arridge and M. Schweiger. Photon-measurement density functions. Part 2: Finite-element-method calculations. *Appl. Opt.* **34**, 8026-8037 (1995).

[80] S. R. Arridge and M. Schweiger. Direct calculation of the moments of the distribution of photon time of flight in tissue with a finite-element method. *Appl. Opt.* **34**, 2683-2687 (1995).

[81] M. Schweiger and S. R. Arridge. Direct calculation with a finite-element method of the Laplace transform of the distribution of photon time of flight in tissue. *Appl. Opt.* **36**, 9042-9049 (1997).

[82] S. R. Arridge and M. Schweiger. A general framework for iterative reconstruction algorithms in optical tomography, using a finite element method. *Computational Radiology and Imaging: Therapy and Diagnosis* (Ed. C. Borgers and F. Natterer) *IMA Volumes in Mathematics and its Applications* (1998).

[83] M. Schweiger and S. R. Arridge. Comparison of two- and three-dimensional reconstruction methods in optical tomography. *Appl. Opt.* **37**, 7419-7428 (1998).

[84] M. Schweiger and S. R. Arridge. Application of temporal filters to time resolved data in optical tomography. *Phys. Med. Biol.* **44**, 1699-1717 (1999).

[85] A. P. Gibson, J. Riley, M. Schweiger, J. C. Hebden, S. R. Arridge, and D. T. Delpy. A method for generating patient-specific finite element meshes for head modeling. *Phys. Med. Biol.* **48**, 481-495 (2003).

[86] K. D. Paulsen and H. Jiang. Spatially varying optical property reconstruction using finite element diffusion equation approximation. *Med. Phys.* **22**, 691-701 (1995).

[87] H. Jiang, K. D. Paulsen, and U. L. Östenberg. Optical image reconstruction using DC data: simulations and experiments. *Phys. Med. Biol.* **41**, 1483-1498 (1996).

[88] H. Jiang, K. D. Paulsen, U. L. Ostenberg, B. W. Pogue, and M. S. Patterson. Optical image reconstruction using frequency-domain data: simulations and experiments. *J. Opt. Soc. Am. A* **13**, 253-266 (1996).

[89] N. Iftimia and H. Jiang. Quantitative optical image reconstruction of turbid media by use of direct-current measurements. *Appl. Opt.* **39**, 5256-5261 (2000).

[90] A. Y. Bluestone, G. Abdoulaev, C. H. Schmitz, R. L. Barbour, and A. H. Hielscher. Three-dimensional optical tomography of hemodynamics in the human head. *Opt. Expr.* **9**, 272-286 (2001).

[91] R. L. Barbour, H. L. Graber, Y. Pei, S. Zhong, and C. H. Schmitz. Optical tomographic imaging of dynamic features of dence-scattering media. *J. Opt. Soc. Am. A* **18**, 3018-3036 (2001).

[92] V. Kolehmainen, S. R. Arridge, W. R. B. Lionheart, M. Vauhkonen, and J. P. Kaipio. Recovery of region boundaries of piecewise constant coefficients of an elliptic PDE from boundary data. *Inv. Probl.* **15**, 1375-1391 (1999).

[93] F. Gao, P. Poulet, and Y. Yamada. Simultaneous mapping of absorption and scattering coefficients from a three-dimensional model of time-resolved optical tomography. *Appl. Opt.* **39**, 5898-5910 (2000).

[94] B. C. Wilson and G. Adam. A Monte Carlo model for the absorption and flux distributions of light in tissue. *Med. Phys.* **10**, 824-830 (1983).

[95] S. A. Prahl, M. Keijzer, S. L. Jacques, and A. J. Welch. A Monte Carlo model of light propagation in tissue. *SPIE Institute Series* **5**, 102-111 (1989).

[96] M. Bonnet. *Boundary Integral Equation Methods for Fluids and Solids* (J. Wiley and Sons, 1999).

[97] A. A. Becker. *The Boundary Element Method in Engineering. A complete course* (McGraw–Hill Book Company, 1992).

[98] G. Beer. *Programming the Boundary Element Method. An Introduction for Engineers* (J. Wiley and Sons, 2001).

[99] M. Hiraoka, M. Firbank, M. Essenpreis, M. Cope, S. R. Arridge, P. van der Zee, and D. T. Delpy. A Monte Carlo investigation of optical pathlength in inhomogeneous tissue and its application to near-infrared spectroscopy. *Phys. Med. Biol.* **38**, 1859-1876 (1993).

[100] S. R. Arridge and W. R. B. Lionheart. Nonuniqueness in diffusion-based optical tomography. *Opt. Lett.* **23**, 882-884 (1998).

[101] R. Kohn and M. Vogelius. Determining conductivity by boundary measurements II Interior results. *Comm. Pure. Appl. Math.* **38**, 643-667 (1985).

[102] J. Sylvester. An anisotropic inverse boundary value problem. *Comm. Pure Appl. Math.* **43**, 201-232 (1990).

[103] B. J. Tromberg, N. Shah, R. Lanning, A. Cerussi, J. Espinoza, T. Pham, L. Svaasand, and J. Butler. Non-invasive *in vivo* characterization of breast tumors using photon migration spectroscopy. *Neoplasia* **2**, 1-15 (2000).

[104] Å. Björck. *Numerical Methods for Least Squares Problems* (SIAM, Philadelphia, 1996).

[105] J. E. Dennis and R. B. Schnabel. *Numerical Methods for Unconstrained Optimization and Nonlinear Equations* (SIAM, Philadelphia, 1996).

[106] C. T. Kelley. *Iterative Methods for Optimization* (SIAM, electronic version, 1999).

[107] P. C. Hansen. *Rank-Deficient and Discrete Ill-Posed Problems - Numerical Aspects of Linear Inversion* (SIAM Monographs on Methematical Modeling and Computation, 1998).

[108] J. P. Kaipio and E. Somersalo. *Computational and Statistical Methods for Inverse Problems* (Applied Mathematical Sciences 160, Springer-Verlag, New York, ISBN 0-387-22073-9, 2004).

[109] J. J. Stott, J. P. Culver, S. R. Arridge, and D. A. Boas. Optode positional calibration in diffuse optical tomography. *Appl. Opt.* **42**, 3154-3162 (2003).

[110] D. A. Boas, T. Gaudette, and S. R. Arridge. Simultaneous imaging and optode calibration with diffuse optical tomography. *Opt. Exp.* **8**, 263-270 (2001).

[111] T. Tarvainen, V. Kolehmainen, M. Vauhkonen, A. Vanne, J. P. Kaipio, A. P. Gibson, S. R. Arridge, and M. Schweiger. Computational calibration method for optical tomography. *Appl. Opt.* **44**, 1879-1888 (2005).

ISBN 951-22-7668-2
ISBN 951-22-7669-0 (PDF)
ISSN 1795-2239
ISSN 1795-4584 (PDF)